# CHAPTER 7

# ANALYSES OF THE AXIAL LOAD TESTS AT THE ROUTE 351 BRIDGE

## 7.1 INTRODUCTION

In this chapter, calculations using methods commonly employed in practice are presented for the pile axial load capacity, and for the load-deflection behavior, of the three test piles at the Route 351 Bridge project. The calculations are compared with the recorded pile capacities and the measured load-deflection responses. Background information for the methodologies used to perform the analyses are also presented and discussed in this chapter.

## 7.2 AXIAL PILE CAPACITY

### 7.2.1 Methods to estimate axial load capacity of driven piles in sand

The axial capacity of driven piles in sand is possibly the area of greatest uncertainty in foundation design (Randolph et al. 1994), and many methods are available for predicting pile capacity. Despite the extensive amount of research in this area, the appropriateness and accuracy of current design methods is often questioned (Randolph et al. 1994, Olson 2002). In practice it is common to use factors of safety of two, three, or more since measured pile capacities of driven piles have been found to differ from the calculated capacities by more than three times (Olson 2002). It is expected that these uncertainties will be applicable to driven composite piles. With this in mind, the predictions for the composite piles presented in this chapter are expected to show at best a level of accuracy similar to the predictions for conventional piles.

The predictions presented herein are based primarily on design methods commonly used by U.S. highway agencies, with the exception of a relatively new method proposed by

Jardine and others at the Imperial College in England, which seems to provide a rational approach for assessing axial load capacity of driven piles (Jardine and Chow 1996).

A sketch of the axially loaded pile problem is shown in Figure 7.1. Generally, most methods estimate the ultimate pile capacity based on consideration of vertical equilibrium of the pile at the state of incipient bearing capacity failure (i.e., when the settlement of the pile increases rapidly with little further increase in load at the pile head). From Figure 7.1, the ultimate axial capacity of a pile is given by the equation:

$$Q_T = Q_s + Q_b - W_p \tag{7.1}$$

where $Q_T$ is the estimated ultimate axial capacity, $Q_s$ is the ultimate shaft capacity resulting from the surrounding soil in side shear, $Q_b$ is the total ultimate tip load at the base or tip of the pile (total indicates the weight of the displaced volume of soil is included), and $W_p$ is the weight of the pile. In practice, the term $W_p$ is usually neglected since it is considered small compared to the accuracy of the prediction of $Q_T$.

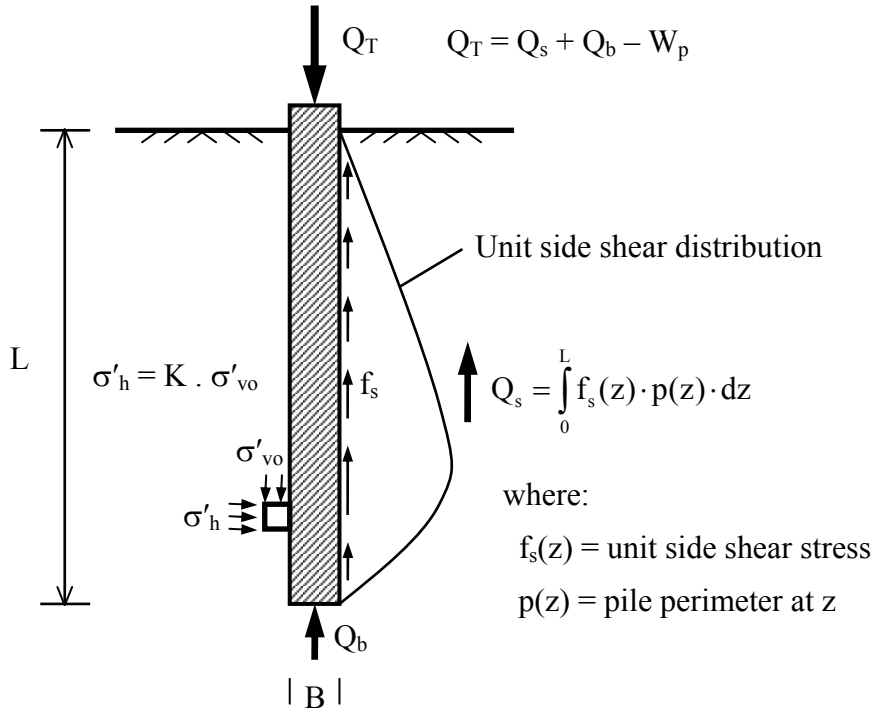


**Figure 7.1. Load Transfer in an Axially Loaded Pile**

The load capacity contributed by the shaft side shear, $Q_s$, is calculated by integrating the side shear stresses along the pile embedded length:

$$Q_s = \int_0^L f_s(z) \cdot p(z) \cdot dz \tag{7.2}$$

where $f_s(z)$ is the shear stress between the pile and the soil at a depth z, p(z) is the pile perimeter at depth z, and L is the embedment depth of the pile.

The expression used for the tip or end bearing of the pile is usually of the form:

$$Q_b = A_b \cdot q_b \tag{7.3}$$

where $A_b$ is the tip or end area of the pile, and $q_b$ is the total ultimate end-bearing or tip stress.

The different pile capacity methods deal with ways of estimating the side friction, $f_s$, and the ultimate end-bearing stress, $q_b$. The following sections will summarize the most common methods used in practice to estimate $f_s$ and $q_b$ for piles driven in sands.

#### 7.2.1.1 Nordlund's method

This method is often used in U.S. highway agencies and is advocated by the FHWA (Olson 2002). The Nordlund method is a semi-empirical method based on a database of pile load tests (Nordlund 1963, 1979). The method accounts for differences in soil-pile interface for different piles. For the sake of brevity, only the most pertinent details of the method are presented. A complete description of this method can be found in Hannigan et al. (1996).

According to the Nordlund method, the shaft shear stress, $f_s$, of a uniform cross section pile, embedded a length L can be estimated as follows (Hannigan et al. 1996):

$$f_s = K_\delta \cdot C_F \cdot \sigma'_v(z) \cdot \sin\delta \quad (7.4)$$

where: $K_\delta$ = coefficient of lateral earth pressure,
$C_F$ = correction factor for $K_\delta$ when $\delta \neq \phi$,
$\sigma'_v(z)$ = free-field effective overburden pressure at depth z,
$\delta$ = interface friction angle between pile and soil.

As pointed out by Olson (2002), the term $\sigma'_v(z)$ in Equation 7.4 should, rigorously speaking, correspond to the effective vertical stress at depth z, right next to the pile shaft. Because this stress is unknown, it is common to use the free-field vertical stress which corresponds to the in-situ value far away from the influence of the pile.

The expression proposed by Nordlund for the ultimate end-bearing stress, $q_b$, is as follows:

$$q_b = \alpha_T \cdot N'_q \cdot \sigma'_v(z = L) \quad (7.5)$$

where: $\alpha_T$ = dimensionless factor dependent on pile depth-width ratio,
$N'_q$ = bearing capacity factor (function of $\phi'$),
$\sigma'_v(z = L)$ = free-field effective overburden pressure at the pile tip (z = L).

Values for the coefficients $K_\delta$, $C_F$, $N'_q$, $\alpha_T$, and for the interface friction angle $\delta$, are typically read from design charts found in the technical literature, such as the FHWA manual for driven piles (Hannigan et al. 1996).

#### 7.2.1.2 API method

The American Petroleum Institute (API) provides design recommendations for axially loaded piles in the API RP 2A publication: "Recommended Practice for Planning, Designing, and Constructing Fixed Offshore Platforms" (API 1993). Although this method is not as commonly used as the Nordlund method by highway agencies, it is worth presenting here because the recommendations of API are based on a large database of axial pile load tests that is continually evaluated and updated (Pelletier et al. 1993).

According to API (1993) the shaft shear for piles in sands can be estimated using:

$$f_s(z) = \sigma'_v(z) \cdot K \cdot \tan(\delta) \qquad (7.6)$$

where: $\sigma'_v(z)$ = free-field effective overburden pressure at depth z,
K = earth pressure coefficient,
$\delta$ = interface friction angle between pile and soil (as per Table 7.1).

API (1993) recommends using a value for the earth pressure coefficient, K, of 1.0 for full displacement piles, such as the piles tested in this project. Equation 7.6 implies that the shaft friction can increase indefinitely with depth, i.e., with increasing effective overburden pressure. However, API recommends using limiting values for $f_s$, as shown in Table 7.1. In the absence of interface friction angle test data, API recommends using the values of soil-pile interface friction angles, $\delta$, listed in Table 7.1.

**Table 7.1. API Recommendations for Side Friction in Siliceous Soil (API 1993) [1]**

| Density | Soil description | Soil-pile interface friction angle, $\delta$ [2] (degrees) | Limiting shaft friction, $f_s$ | |
|---|---|---|---|---|
| | | | (kips/ft$^2$) | (kPa) |
| Very loose | Sand | 15 | 1.0 | 47.8 |
| Loose | Sand-silt [3] | | | |
| Medium | Silt | | | |
| Loose | Sand | 20 | 1.4 | 67.0 |
| Medium | Sand-silt | | | |
| Dense | Silt | | | |
| Medium | Sand | 25 | 1.7 | 81.3 |
| Dense | Sand-silt | | | |
| Dense | Sand | 30 | 2.0 | 95.7 |
| Very dense | Sand-silt | | | |
| Dense | Sand | 35 | 2.4 | 114.8 |
| Very dense | Sand-silt | | | |

Notes: 1) These values provided by API are intended as guidelines only, and where detailed information is available other values may be justified.
2) Suggested values are for steel pipe piles driven in cohesionless soils.
3) Sand-silt is described as soils with significant fraction of both sand and silt.

API recommends using the following expression to estimate the ultimate end-bearing or tip resistance for piles driven in sands:

$$q_b = \sigma'_v(z = L) \cdot N_q \tag{7.7}$$

where: $\sigma'_v(z = L)$ = free-field effective overburden pressure at the pile tip (z = L), $N_q$ = bearing capacity factor (as per Table 7.2).

Similarly to $f_s$, API recommends limiting the value of the tip resistance, $q_b$. The recommended values of $N_q$ and limiting $q_b$ are shown in Table 7.2.

**Table 7.2. API Recommendations for Tip resistance in Siliceous Soil (API 1993)**

| Density | Soil description | $N_q$ | Limiting tip resistance, $q_b$ | |
|---|---|---|---|---|
| | | | (kips/ft$^2$) | (MPa) |
| Very loose | Sand | 8 | 40 | 1.9 |
| Loose | Sand-silt | | | |
| Medium | Silt | | | |
| Loose | Sand | 12 | 60 | 2.9 |
| Medium | Sand-silt | | | |
| Dense | Silt | | | |
| Medium | Sand | 20 | 100 | 4.8 |
| Dense | Sand-silt | | | |
| Dense | Sand | 40 | 200 | 9.6 |
| Very dense | Sand-silt | | | |
| Dense | Sand | 50 | 250 | 12.0 |
| Very dense | Sand-silt | | | |

### 7.2.1.3 LCPC method

The Laboratoire Central des Ponts et Chaussees (LCPC) method estimates pile capacities based on CPT tip resistance ($q_c$) values (Bustamante and Gianeselli 1982). A detailed description of the method can be found in (Lunne et al. 1997).

The unit shaft resistance, $f_s$, is determined based on the pile type, installation method, and the value of the CPT tip resistance, $q_c$. The recommended pile shaft resistance is obtained by dividing the measured $q_c$ by a friction coefficient $\alpha_{LCPC}$. A limiting shaft friction is recommended based on pile and soil type. The values of recommended friction coefficients, $\alpha_{LCPC}$, and maximum limit of $f_s$ for driven piles in sands are summarized in Table 7.3.

**Table 7.3. LCPC Friction Coefficient, $\alpha_{LCPC}$ for Driven Piles in Sands (Bustamante and Gianeselli 1982)**

| State of sand | $q_c$ (MPa) | Pile Category | | | |
|---|---|---|---|---|---|
| | | Coefficient, $\alpha_{LCPC}$ | | Maximum limit of $f_s$ (MPa) | |
| | | Concrete | Steel | Concrete | Steel |
| Loose | ≤ 5 | 60 | 120 | 0.035 | 0.035 |
| Medium dense | 5 to 12 | 100 | 200 | 0.08 | 0.08 |
| Dense to very dense | > 12 | 150 | 200 | 0.12 | 0.12 |

The LCPC method correlates the pile unit tip resistance, $q_b$, to an equivalent average cone resistance, $q_{ca}$, calculated using the $q_c$ values within 1.5 pile diameters (or widths) below and above the pile tip elevation, as described by Lunne et al. (1997). The LCPC pile tip resistance, $q_b$, is calculated by multiplying the equivalent average cone resistance, $q_{ca}$, by an end bearing coefficient, $k_c$. The recommended values for end bearing factors for driven piles in sands are summarized in Table 7.4.

**Table 7.4. LCPC Bearing Capacity Factors for Driven Piles in Sands (Bustamante and Gianeselli 1982)**

| State of sand | $q_c$ (MPa) | Factor $k_c$ |
|---|---|---|
| Loose | $\leq 5$ | 0.5 |
| Medium dense | 5 to 12 | 0.5 |
| Dense to very dense | > 12 | 0.4 |

#### 7.2.1.4 Imperial College method

This method was developed at the Imperial College, in London, England, by Jardine and his colleagues based on a series of investigations using instrumented field test piles (Jardine 1985, Bond 1989, Lehane 1992, and Chow 1996). The instrumented piles were tubular closed and open-ended steel piles driven in sands for supporting offshore structures used in the oil industry.

The major findings of the Imperial College experiments, related to piles driven in sands, are summarized below (Jardine and Lehane 1993, Jardine and Chow 1996):

- The peak local shaft friction ($f_s$) is related to the local radial effective stress at failure ($\sigma'_{rf}$) by the following simple Mohr-Coulomb effective stress criterion:

$$f_s = \sigma'_{rf} \cdot \tan \delta_f \tag{7.8}$$

where: $\sigma'_{rf}$ = the local radial effective stress at failure
$\delta_f = \delta_{cv}$ = failure or constant volume interface friction angle

- The radial effective stresses developed around the pile shaft after installation ($\sigma'_{rc}$) were found to depend strongly on the initial relative density of the sand ($D_r$) and the distance to the pile tip from the point where the radial stress is being evaluated. The following empirical expression, based on statistical analyses of over sixty data sets of radial stress, is recommended to estimate the local radial effective stress, $\sigma'_{rc}$, of close-ended piles:

$$\sigma'_{rc}(z) = 0.029 \cdot q_c \cdot \left( \frac{\sigma'_v(z)}{P_a} \right)^{0.13} \cdot \left( \frac{h}{R} \right)^{-0.38} \tag{7.9}$$

where: $\sigma'_{rc}(z)$ = local radial effective stress after installation,
$q_c$ = CPT tip resistance,
z = depth below ground surface,
L = pile embedded length,
h = L-z = distance to pile tip,
$\sigma'_v(z)$ = free-field effective overburden pressure at depth z,
$P_a$ = atmospheric pressure (= 100 kPa),
R = pile radius,
$\frac{h}{R}$ = 8 for points close to the tip where h < 8R.

- Jardine and Lehane (1993) found that the radial stresses could rise considerably (by about 50%) due to localized dilation at the pile-soil interface during axial compression loading of the pile. The radial stresses were found to reach a maximum near the mobilization of the peak shear stresses. The increase in radial effective stresses was found to vary in inverse proportion to the pile radius, and was found to be predicted reasonably well using the simple elastic cylindrical cavity expansion theory proposed by Boulon and Foray (1986).

- Constant volume or residual interface friction angles ($\delta_{cv}$) were found to control the developed peak local shear stresses in pile tests. The values determined from laboratory interface shear tests were found to correlate well with their field test measurements. The interface friction angle was found to depend on sand grain size, shape, and mineral type. The pile material hardness and surface roughness were also found to influence $\delta$. Jardine and co-workers pointed out that the level of radial effective stress may also influence $\delta$, but they indicated that more research is needed to investigate this further.

The Imperial College (IC) method provides a simple, practical, and rational approach to predict pile capacity of piles driven in sands. A complete description of the IC design method can be found in Jardine and Chow (1996), and a brief description is presented here.

The basic steps involved in the IC method to estimate the shaft capacity of closed-ended driven piles in sands are:

1. Calculate the local radial effective stress around the pile after pile installation, $\sigma'_{rc}$ using Equation 7.9,

2. Calculate the increase in radial effective stresses, $\Delta\sigma'_{rd}$, due to dilation during pile loading. Jardine and Chow (1996) recommend using the following expression based on cylindrical cavity expansion theory:

$$\Delta\sigma'_{rd} = 2 \cdot G \cdot \frac{\delta h}{R} \tag{7.10}$$

where: G = operational shear modulus of sand (see note below),
$\delta h$ = average radial displacement (see note below),
R = pile radius.

Notes:

- G:

  Since the shear stiffness of sands is nonlinear, pressure dependent, and anisotropic, the method recommends using reliable and appropriate measurements of the shear modulus. If these measurements are not available, the following expression (after Chow 1996) is recommended:

$$G = \frac{q_c}{[A + B \cdot \eta - C \cdot \eta^2]}$$

and,

$$\eta = \frac{q_c}{\sqrt{P_a \cdot \sigma'_v}} \tag{7.11}$$

  where: $q_c$ = CPT tip resistance,
  A = 0.0203,
  B = 0.00125,
  C = 1.216 x $10^{-6}$,
  $\sigma'_v$ = free-field effective overburden pressure,
  $P_a$ = atmospheric pressure (100 kPa).

- $\delta h$:

  The term $\frac{\delta h}{R}$, in equation 7.10, comes from cylindrical cavity expansion theory, and corresponds to the cavity strain. The term $\delta h$ refers to radial sand dilation, and can be estimated as being equal to the average peak-to-trough height obtained from surface roughness measurements of the pile (Chow 1996). The average peak to trough height ($R_i$) is equal to twice the centerline average roughness parameter ($R_{cla}$). $R_{cla}$ is a surface roughness parameter commonly

used by material scientists, and it is defined as the average distance of peaks and troughs to the surface profile centerline taken over an 8 mm gauge length.

3. Select the interface friction angle (δ) based on laboratory interface shear tests. Alternatively, δ, can be estimated using published correlations, preferably if developed considering pile material characteristics (roughness and hardness) and sand characteristics (shape, $D_{50}$, mineralogy).

4. Calculate the local radial effective stress at failure, as follows:

$$\begin{aligned} \sigma'_{rf} &= \sigma'_{rc} + \Delta\sigma'_{rd} \quad \text{(for compression loading)} \\ \sigma'_{rf} &= 0.8 \cdot \sigma'_{rc} + \Delta\sigma'_{rd} \quad \text{(for tension loading)} \end{aligned} \tag{7.12}$$

where: $\sigma'_{rc}$ from Step 1 using Equation 7.9,

$\Delta\sigma'_{rd}$ from Step 2 using Equation 7.10

5. Calculate the local shear stresses using Equation 7.8.

6. Determine the shaft capacity by integrating the local shear stresses (obtained in Step 4) along the embedded shaft length.

The IC method defines the tip resistance as the total utilizable tip resistance at a pile head displacement equal to 10 % of the pile diameter. The recommended pile base resistance for closed-ended, driven, piles in sand, is related to the CPT tip resistance, $q_c$, averaged near the pile tip, according to the following empirical equation:

$$q_b = \overline{q}_c \cdot \left[ 1 - 0.5 \cdot \log_{10}\left( \frac{D}{D_{CPT}} \right) \right] \geq 0.13 \cdot \overline{q}_c \tag{7.13}$$

where: $\overline{q}_c$ = is the CPT tip resistance averaged over 1.5 pile diameters above and below the pile tip,
D = the pile diameter,
$D_{CPT}$ = 0.036 m = the CPT diameter.

The above equation is based on IC pile load test data that showed that the measured profiles of pile tip resistance, $q_b$, fell close to the CPT $q_c$ traces. The ratio $q_b/q_c$ was found to be less than unity and to decrease with pile diameter (Jardine and Chow 1996). Equation 7.13 tends to zero at D = 3.6 m, therefore a lower bound value of $q_b = 0.13 \cdot \overline{q}_c$ is recommended for D > 2m.

### 7.2.2 Predicted axial capacities

Predictions for the three piles tested at the Route 351 project were made using the four methods described in Section 7.2.1. The predictions presented in the following sections were based on the geotechnical investigation results presented in Chapter 6, and the interpreted average CPT and SPT design profiles, shown in Figure 7.2. The predictions for each pile type included the specific information for each pile capacity prediction method. Pile specific information included: cross-sectional shape and dimensions, embedment depths, surface roughness, and interface friction values.

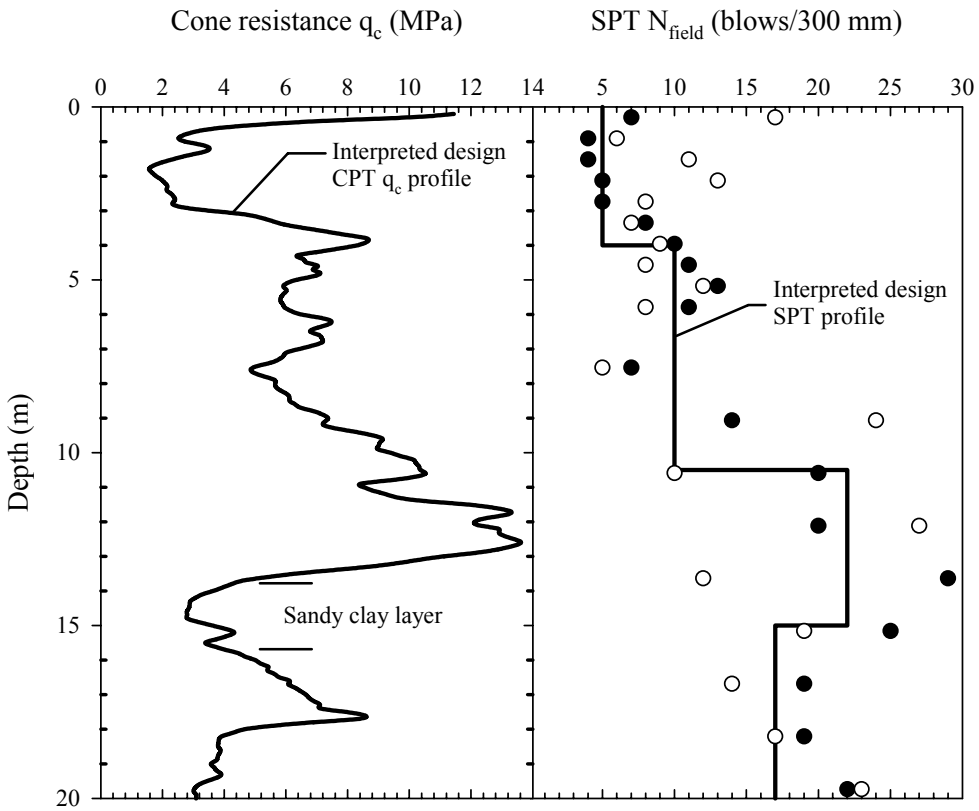


**Figure 7.2 Interpreted Average CPT and SPT Design Profiles for Rte 351 test site**

### 7.2.2.1 Nordlund method predictions

Two sets of axial capacity predictions were made using the Nordlund method. One set of predictions were carried out using the recommended values of δ read directly from the Nordlund design charts. The curve for concrete was used for the prestressed concrete pile, and the curve for steel was used for the composite piles. The second set of Nordlund method predictions used the constant volume interface friction angles, $\delta_{cv}$, obtained in this research, as presented in Chapter 3. The two sets of axial pile capacity predictions using the Nordlund method are compared to the measured pile capacities evaluated from the load test results using the Davisson's failure criterion in Figures 7.3 and 7.4.

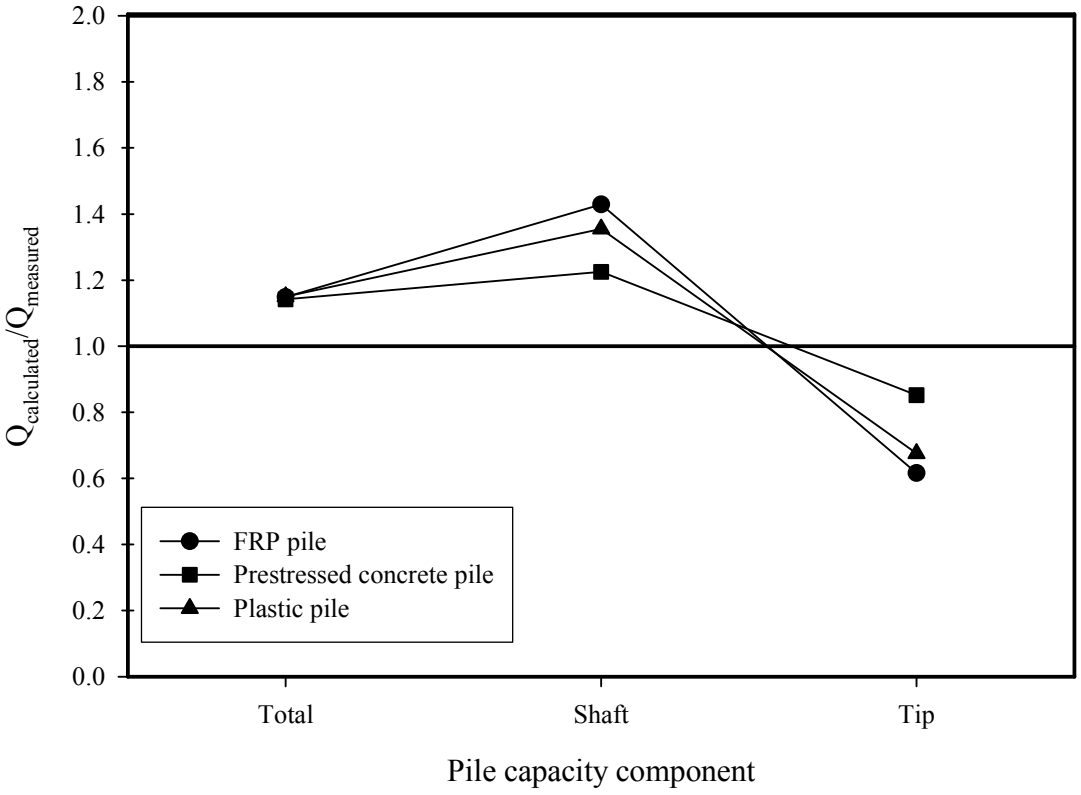


**Figure 7.3 Accuracy of Nordlund method predictions using δ values from Nordlund's charts**

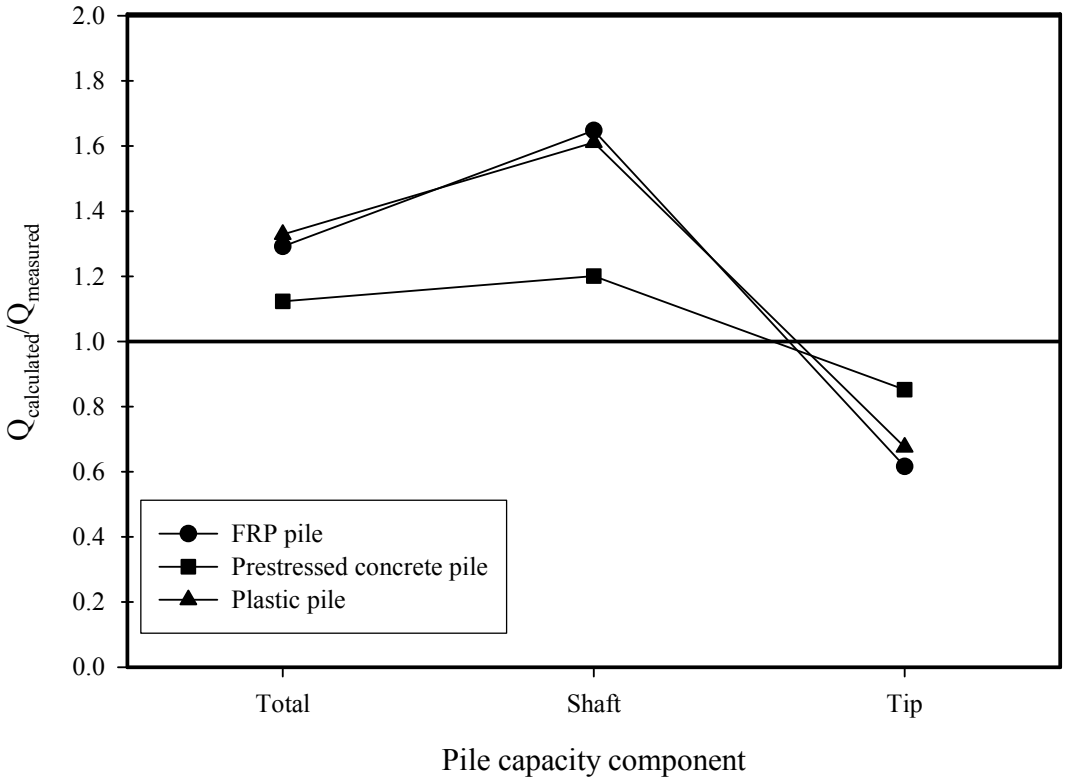


**Figure 7.4 Accuracy of Nordlund method predictions using δ values from interface shear tests**

Figures 7.3 and 7.4 show that the tip capacities ($Q_b$) were under-predicted by about 35 percent for the composite piles and 15 percent for the prestressed concrete pile. The shaft capacities were over-predicted in both sets of predictions. The shaft capacities predicted using Nordlund's recommended interface friction angles, using the steel curve for the composite piles, were 35 to 43 percent higher than measured for the composite piles and 23 percent higher for the prestressed concrete pile. The shaft capacities calculated using the δ values from interface shear tests were about 65 percent higher for the composite piles and 20 percent higher for the prestressed concrete pile. The average coefficient of lateral earth pressure, $K_\delta$, from the Nordlund method, was about 1.67. This value of $K_\delta$ may be over-predicting the effective radial normal stresses acting at the pile-soil interface, hence producing higher shaft capacities than measured. In order to match the shaft capacities from the pile load tests, the coefficient of lateral earth pressure, $K_\delta$,

would have to be around 1.0 for the composite piles and about 1.4 for the prestressed concrete pile, when using the δ values from the interface shear tests.

#### 7.2.2.2 API method predictions

Two sets of axial capacity predictions were made using the API (1993) method. One set of predictions was carried out using API's recommended value of δ from Table 7.1. The second set of API method predictions used the constant volume interface friction angles, $\delta_{cv}$, from the interface shear tests presented in Chapter 3. Comparisons of the two API predictions and the measured pile capacities are shown in Figures 7.5 and 7.6.

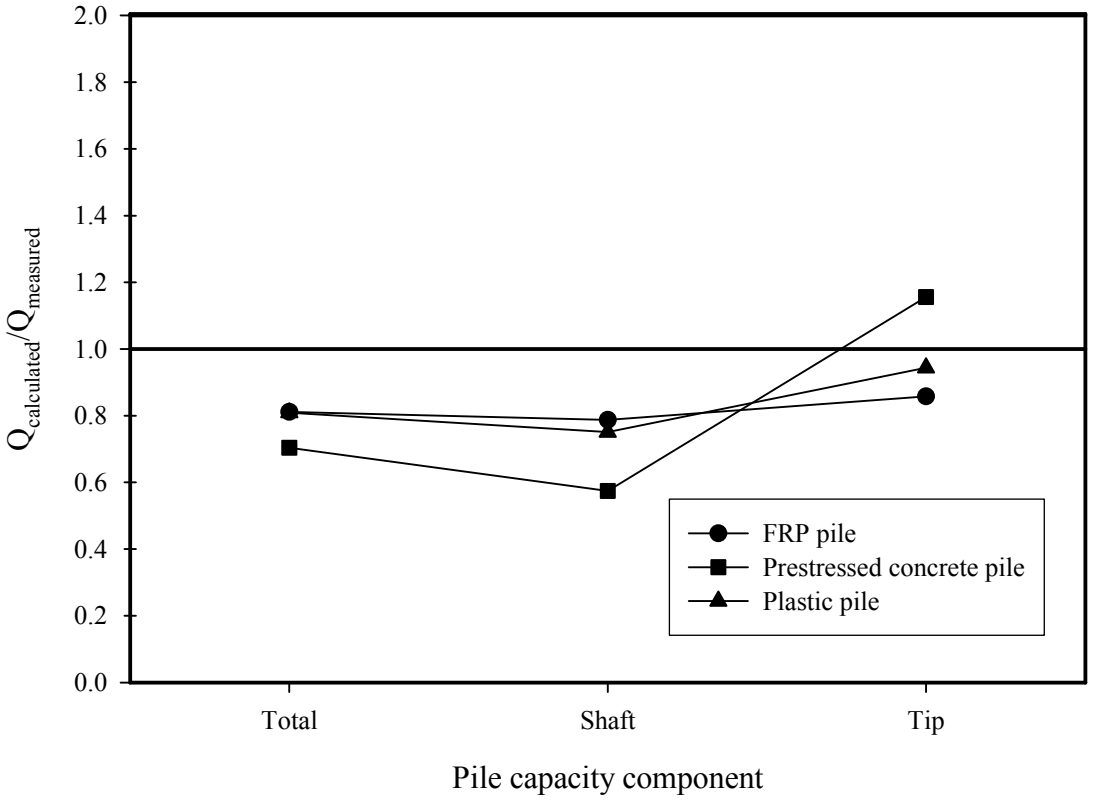


**Figure 7.5 Accuracy of API method predictions using δ values from Table 7.1**

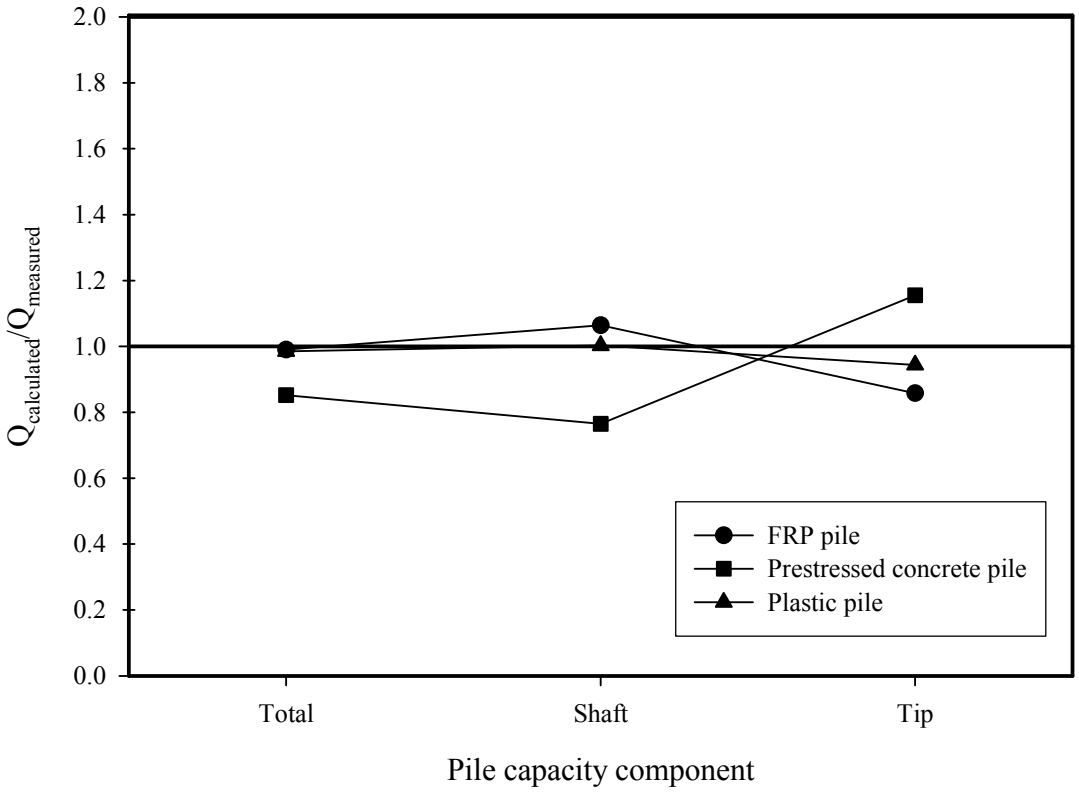


**Figure 7.6 Accuracy of API method predictions using δ values from interface shear tests**

The tip capacities ($Q_b$) predicted for the three piles, using the API method, were within ± 15 percent of the measured values, based on the Davisson failure criterion. The shaft capacities estimated using the API recommended interface friction angles, which are for steel pipe piles, were about 23 percent lower than measured for the composite piles and 43 percent lower for the prestressed concrete pile. The shaft capacities estimated using the δ values from the interface shear tests were between 0.3 and 6 percent higher for the composite piles and 23.5 percent lower for the prestressed concrete pile. The average coefficient of lateral earth pressure, K, from the API method, is 1.0. This value of K, coupled with the δ values from the interface shear tests, resulted in very reasonable predictions of the pile shaft capacities for the composite piles.

### 7.2.2.3 LCPC method predictions

Axial capacity predictions using the LCPC method (Bustamante and Gianeselli 1982) were based on the average obtained from applying the method to the CPT tip resistance, $q_c$, data available at the test site, except that probe CPT-2 was excluded because it produced anomalous data in the depth range of 3 to 8 m. For each pile type, two LCPC capacity calculations were performed: one assumes the particular pile under consideration is a steel pile, and the other assumes the pile is a concrete pile. Comparisons of the measured pile capacities and the LCPC predictions using the steel and concrete pile assumptions are shown in Figures 7.7 and 7.8, respectively.

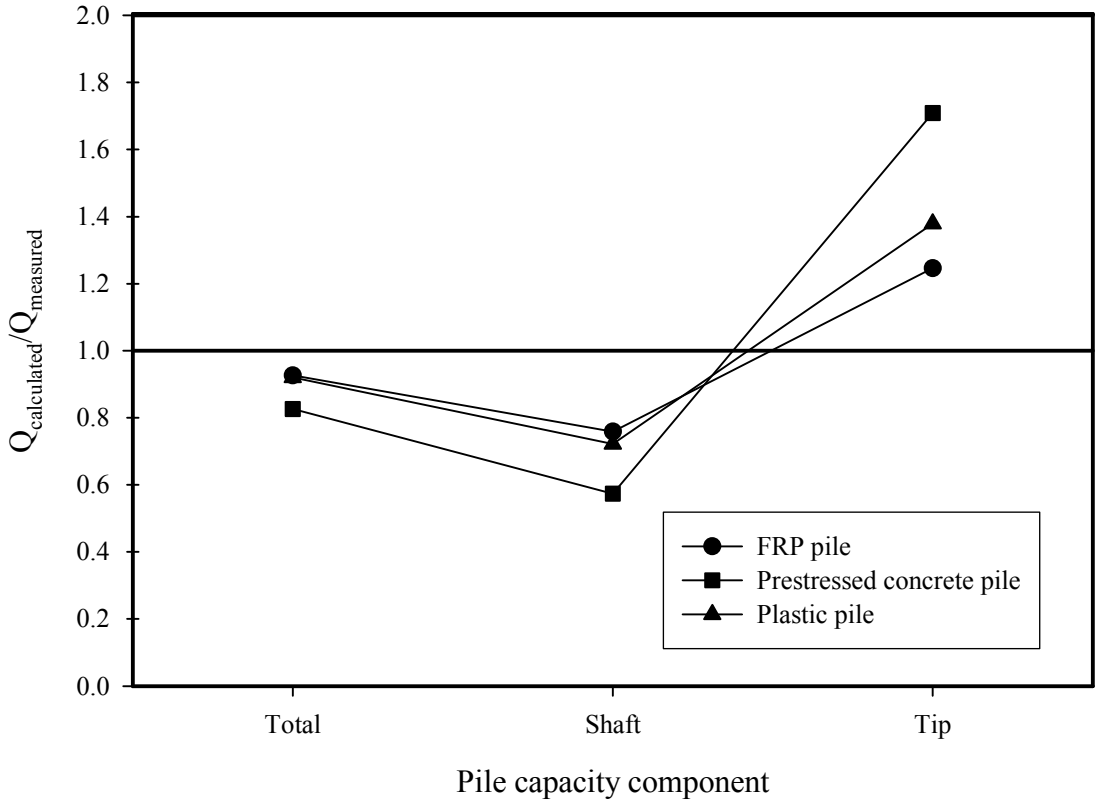


**Figure 7.7 Accuracy of LCPC method predictions using "steel pile" assumption**

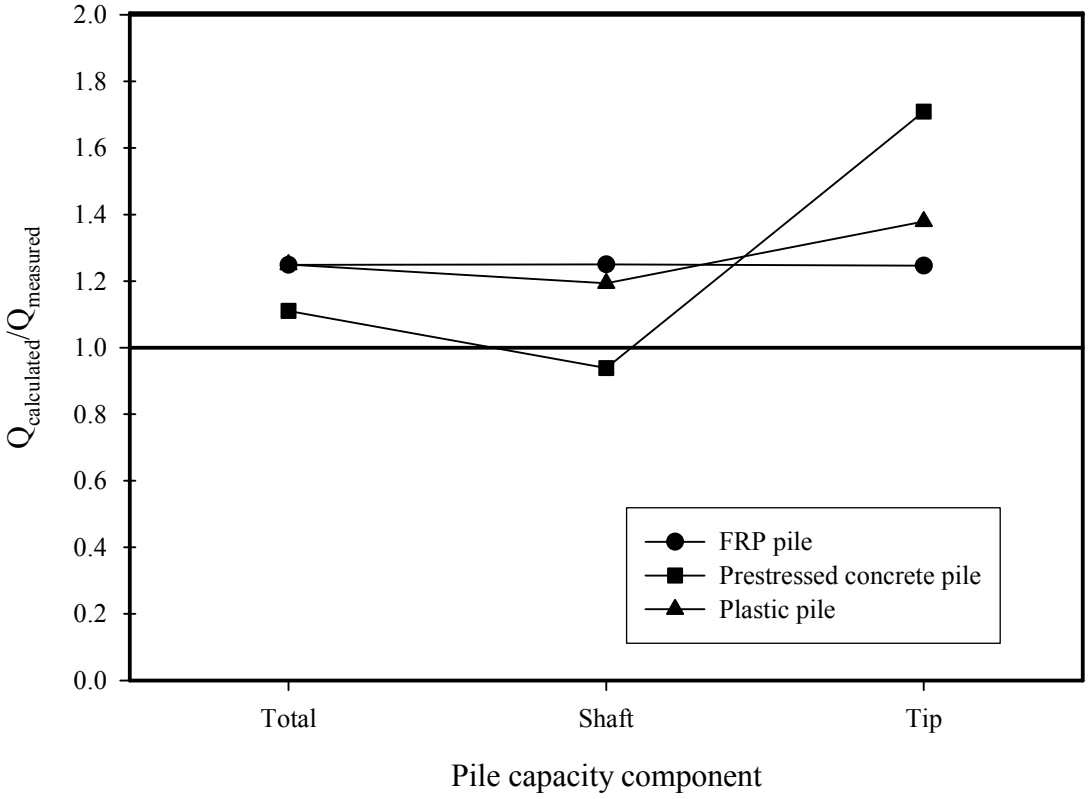


**Figure 7.8 Accuracy of LCPC method predictions using "concrete pile" assumption**

The tip capacities, $Q_b$, estimated using the LCPC method over-predicted the test results by 25 and 38 percent for the composite piles and by 71 percent for the prestressed concrete pile. The shaft capacities estimated using the LCPC "steel pile" approach were 24 and 28 percent lower than measured for the composite piles and 43 percent lower for the prestressed concrete pile. The shaft capacities estimated using LCPC "concrete pile" approach were 19 and 25 percent higher than measured for the composite piles and 6 percent lower for the prestressed concrete pile.

#### 7.2.2.4 Imperial College method predictions

The Imperial College method (Jardine and Chow 1996) was used to predict the axial capacities of the three test piles using the average interpreted design CPT tip resistance ($q_c$) profile shown in Figure 7.2, and the interface friction angle and surface roughness

data presented in Chapter 3. Comparisons of the measured pile capacities and the Imperial College predictions are shown in Figure 7.9.

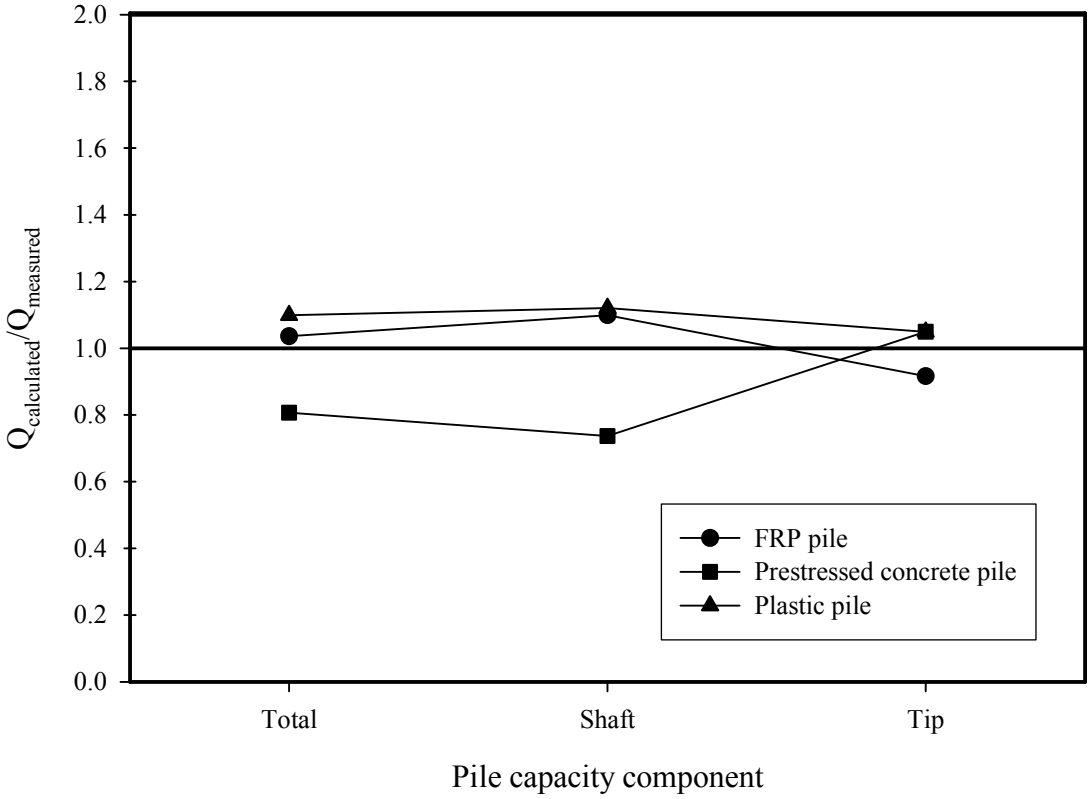


**Figure 7.9 Accuracy of IC method predictions using δ values from interface shear tests**

The predicted tip capacities, $Q_b$, using the Imperial College (IC) method were 8 percent below measured for the FRP composite pile, 5 percent above measured for the plastic composite pile, and 5 percent above measured for the prestressed concrete pile. The shaft capacities estimated using the IC approach were 10 and 12 percent higher than measured for the composite piles, and 26 percent lower for the prestressed concrete pile. The level of agreement between measured and calculated capacities is quite good for all cases except the shaft capacity of the prestressed concrete pile.

### 7.2.3 Summary of axial pile capacity predictions

The predicted axial pile capacities presented in the preceding sections are summarized in Table 7.5.

**Table 7.5 Predicted Axial Capacities for the Test Piles at Route 351**

| Pile | Prediction method | Total capacity | | Shaft capacity | | Toe capacity | |
|---|---|---|---|---|---|---|---|
| | | $Q_c$ (kN) | $Q_c/Q_m$ | $Q_c$ (kN) | $Q_c/Q_m$ | $Q_c$ (kN) | $Q_c/Q_m$ |
| PSC | Nordlund (Concrete) | 3480 | 1.12 | 2890 | 1.2 | 590 | 0.85 |
| | Nordlund (w/ IST δ's) | 3530 | 1.14 | 2950 | 1.23 | 590 | 0.85 |
| | API (w/ recommended δ's) | 2180 | 0.7 | 1380 | 0.57 | 800 | 1.16 |
| | API (w/ IST δ's) | 2640 | 0.85 | 1840 | 0.76 | 800 | 1.16 |
| | LCPC - Steel | 2560 | 0.83 | 1380 | 0.57 | 1180 | 1.71 |
| | LCPC - Concrete | 3440 | 1.11 | 2260 | 0.94 | 1180 | 1.71 |
| | Imperial College | 2500 | 0.81 | 1770 | 0.74 | 720 | 1.05 |
| FRP | Nordlund (Steel) | 2920 | 1.29 | 2440 | 1.65 | 480 | 0.62 |
| | Nordlund (w/ IST δ's) | 2600 | 1.15 | 2120 | 1.43 | 480 | 0.62 |
| | API (w/ recommended δ's) | 1830 | 0.81 | 1160 | 0.79 | 670 | 0.86 |
| | API (w/ IST δ's) | 2240 | 0.99 | 1570 | 1.06 | 670 | 0.86 |
| | LCPC - Steel | 2090 | 0.93 | 1120 | 0.76 | 970 | 1.25 |
| | LCPC - Concrete | 2820 | 1.25 | 1850 | 1.25 | 970 | 1.25 |
| | Imperial College | 2340 | 1.04 | 1630 | 1.1 | 710 | 0.92 |
| Plastic | Nordlund (Steel) | 2830 | 1.33 | 2400 | 1.61 | 430 | 0.68 |
| | Nordlund (w/ IST δ's) | 2450 | 1.15 | 2010 | 1.35 | 430 | 0.68 |
| | API (w/ recommended δ's) | 1720 | 0.81 | 1120 | 0.75 | 610 | 0.94 |
| | API (w/ IST δ's) | 2100 | 0.99 | 1490 | 1 | 610 | 0.94 |
| | LCPC - Steel | 1960 | 0.92 | 1070 | 0.72 | 890 | 1.38 |
| | LCPC - Concrete | 2660 | 1.25 | 1770 | 1.19 | 890 | 1.38 |
| | Imperial College | 2340 | 1.1 | 1670 | 1.12 | 670 | 1.05 |

Notes: IST δ's refers to interface friction angles from interface shear tests. $Q_c$ = calculated value (shown with 3 significant digits), $Q_m$ = measured value corresponding to Davisson's failure criterion. $Q_c/Q_m$ = the ratio of calculated to measured.

The various methods used to predict axial pile capacity led to ratios of calculated to measured pile capacities ($Q_c/Q_m$) ranging from 0.70 to 1.14 for the prestressed concrete pile, and from 0.81 to 1.33 for the composite piles. If only the predictions from the Imperial College method and the API method using the δ-values from the interface shear tests are considered, the $Q_c/Q_m$ ratios ranged from 0.81 to 0.85 for the prestressed concrete pile and from 0.99 to 1.10 for the composite piles. In other words, these two methods under-predict the capacity of the prestressed concrete pile by about 20 %, and over-predict the capacities for the composite piles by about 10 %. In routine deep foundation design practice, factors of safety as low as 1.5 are sometimes used, but

typically they are 2.0 or higher. Even a lower bound factor of safety of 1.5 would ensure that the ultimate geotechnical capacity of the composite piles is not exceeded, but it may not be high enough to ensure acceptable deformations of the foundation system.

In summary, it can be seen from the prediction results that the level of accuracy of the predictions is comparable for all three types of piles. In terms of axial pile capacity predictions, the results presented in this chapter seem to indicate that conventional static analysis methods are applicable to composite piles. However, additional case histories would be needed to corroborate and extend this conclusion to other composite pile types and to different soil conditions.

## 7.3 LOAD-SETTLEMENT BEHAVIOR OF AXIALLY LOADED SINGLE PILES

### 7.3.1 Introduction

The settlement of a single pile in soil under compressive axial loading is a function of several factors such as:

- Soil stratigraphy and characteristics (stiffness, density, compressibility, nonlinearity)
- Pile shape and dimensions
- Pile stiffness
- Pile-soil interaction characteristics

Several methods are reported in the literature for computation of load-settlement behavior of a single pile under axial compression loading. The methods are typically divided in the following main categories:

- Elastic methods
- Load transfer (T-Z) methods
- Modified hyperbolic methods
- Numerical techniques (including finite element and finite difference methods)

A good overview of the different techniques available can be found in Poulos (1989). For this study we focus mainly on the load-transfer (T-Z) methodology which is commonly used by the FHWA and US state transportation agencies. This methodology has recently become more accessible to US highway agencies with the release of the FB-Pier program, which uses this technique for settlement calculations of single and pile groups (Hoit et al. 2000). The development of this program was sponsored by FHWA and is distributed freely to US transportation agencies. Other commonly used programs that employ the "T-Z" methodology to analyze settlement of axially loaded single piles include A-Pile (Ensoft 1998), and CAXPILE (Dawkins 1982).

A brief overview of the load-transfer 'T-Z' methodology is provided in the following section.

### 7.3.2 Background of the load transfer method for pile settlement predictions

The load transfer (T-Z) method is probably the most widely used technique to study the problem of single axially loaded piles, and is particularly useful when the soil behavior is clearly non-linear, and/or when the soil surrounding the pile is stratified. This method involves modeling the pile as a series of elements supported by discrete non-linear springs, which represent the resistance of the soil in skin friction (T-Z springs), and a non-linear spring at the pile tip representing the end-bearing ($Q_b$-Z spring). The soil springs are non-linear representations of the soil reaction, T (or $Q_b$ for the pile tip), versus displacement, Z, as shown schematically in Figure 7.10. Assuming the T-Z and $Q_b$-Z curves are available, the axial load-settlement response can be obtained with the aid of a computer program such as FB-Pier.

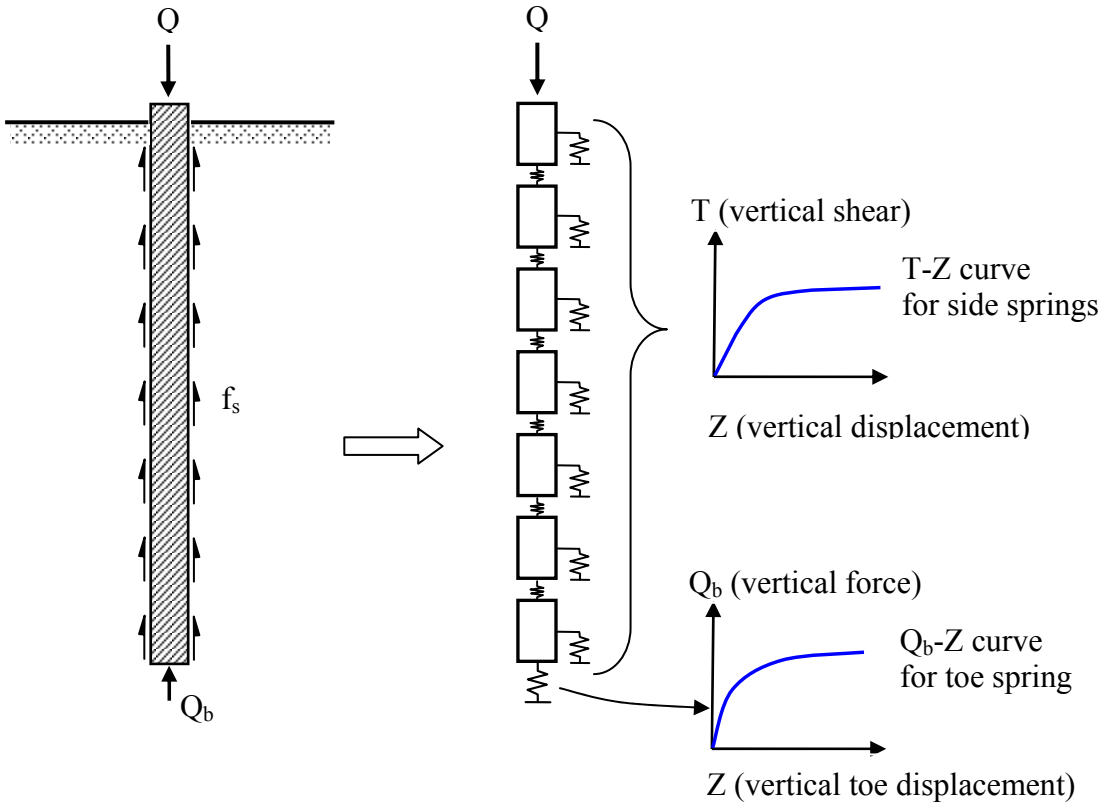


**Figure 7.10 Idealized model used in T-Z load transfer analyses**

Adequate T-Z and $Q_b$-Z curves are essential in this method to obtain reliable settlement and load transfer calculations for axially loaded single piles. Such load transfer curves were originally obtained empirically, e.g., Coyle and Sulaiman (1967) who published empirical T-Z curves based on model and full-scale pile load tests in sand. Building on this work, and based on additional empirical results, general recommendations for estimating T-Z and $Q_b$-Z curves for driven piles in sands have been proposed by Vijayvergiya (1977) and API (1993). Load transfer curves can also be constructed satisfactorily using a theoretical approach related to the shear stiffness of the soil surrounding the pile (Poulos 2001). Several methodologies to develop theoretically based load transfer curves have been proposed, e.g., Kraft et al. (1981), Chow (1986), McVay et al (1989), and Randolph (1994).

Section 7.3.3 presents settlement predictions for the test piles using empirical load transfer curves (API 1993, Vijayvergiya 1977), while Section 7.3.4 presents prediction results using new theoretical load transfer curves.

### 7.3.3 Predictions Using Empirical Load Transfer Curves

#### 7.3.3.1 Predictions using load transfer curves recommended by API (1993)

##### 7.3.3.1.1 Load transfer curves recommended by API (1993)

In the absence of more precise information, API (1993) recommends the use of the following T-Z curve expression (for non-carbonate sands):

$$\begin{aligned} f_s &= f_{s,max} \cdot \frac{z}{z_c} \quad (\text{for } z \le z_c) \\ f_s &= f_{s,max} \quad (\text{for } z > z_c) \end{aligned} \tag{7.13}$$

where: $f_s$ = is the unit side shear stress mobilized along a pile segment at movement, z,

$f_{s,\,max}$ = is the maximum unit side shear stress,

z = movement of pile segment,

$z_c$ = movement required to mobilize $f_{s,\,max}$ (0.1 inches for sands)

In the absence of more definitive criteria, API (1993) recommends using the pile tip load versus tip settlement curve shown in Figure 7.11.

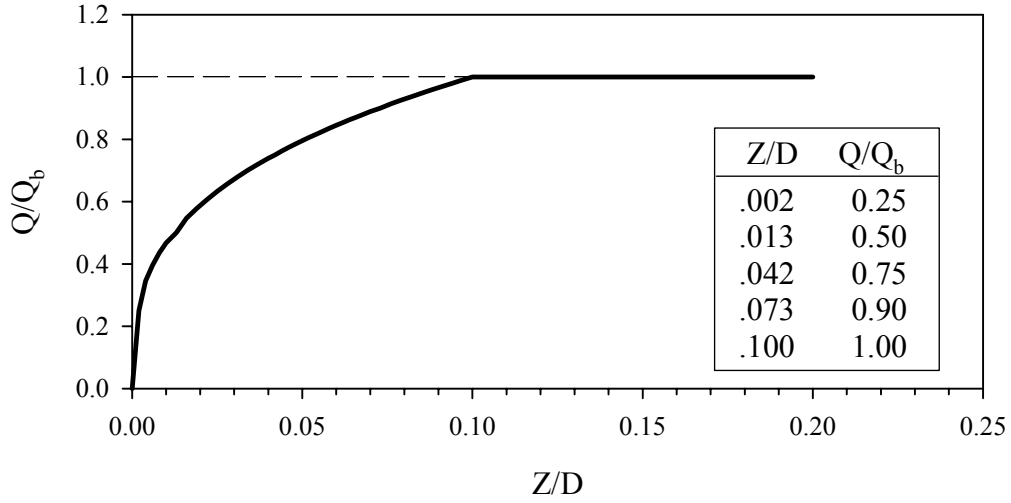


**Figure 7.11 Pile Tip Load – Pile Tip Displacement Curve (Q-Z) (API 1993)**

In Figure 7.11, Q is the mobilized end-bearing capacity at an axial tip displacement z, and $Q_b$ is the ultimate end-bearing load (computed using $q_b$ from Equation 7.7 times the pile tip area). As shown in Figure 7.11, $Q_b$ is mobilized at a pile tip displacement equal to 10 % of the pile diameter, D.

#### 7.3.3.1.2 Maximum shaft shear stress distributions recommended by API (1993)

As described previously in Section 7.2.1.2, API recommends using maximum shear stresses for the pile shaft that increase linearly with depth until they reach a prescribed limiting value. Graphical representations of the maximum shaft shear stresses for the three test piles, as recommended by API (1993), are shown in Figure 7.12. In Section 7.2.3 it was indicated that better pile capacity estimates were obtained using the API method with δ values from interface shear tests. Despite this finding, the shear stresses shown in Figure 7.12 correspond to the δ-values recommended by API (1993). This was done to be able to assess the pile settlement predictions using the original method without major modifications.

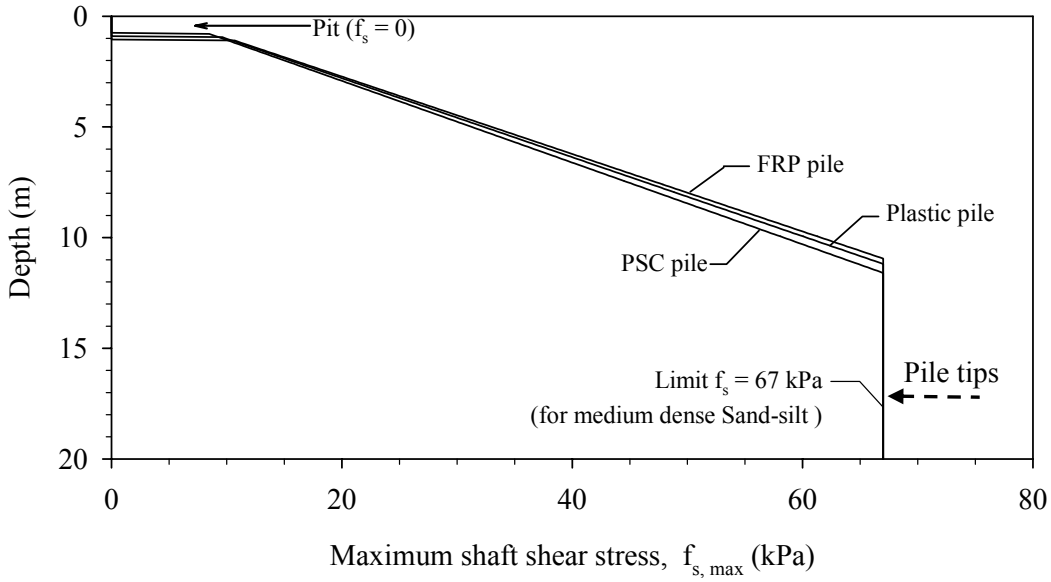


**Figure 7.12 Maximum shear stress distribution along pile shaft, according to API (1993)**

#### 7.3.3.1.3 Prediction for the prestressed concrete test pile

The load-settlement responses predicted for the concrete test pile, using the API (1993) T-Z and $Q_b$-Z curves, are shown in Figure 7.13. The curve showing a lower predicted capacity is based on the API load transfer curves using a limiting shear stress. The second prediction was made using the API curves but without a limiting shaft shear stress.

Figure 7.13 shows that the predicted settlement curves have relatively good agreement in the initial portion of the load settlement curve. However, they both under-predict the measured pile capacity. This is consistent with the axial pile capacity predictions presented in Section 7.2.2.2, where the predicted API pile capacity (using the API recommended δ values) was shown to be about 30 % lower than measured. The predicted load-settlement curve using no limiting $f_s$ shows a slightly better agreement with the field measurements, but also under-predicts the pile capacity by about 18 %.

The extent of this under-prediction is due to the low shaft capacity estimated using API (1993), which as indicated in Section 7.2.2.2, was 43 % lower than measured.

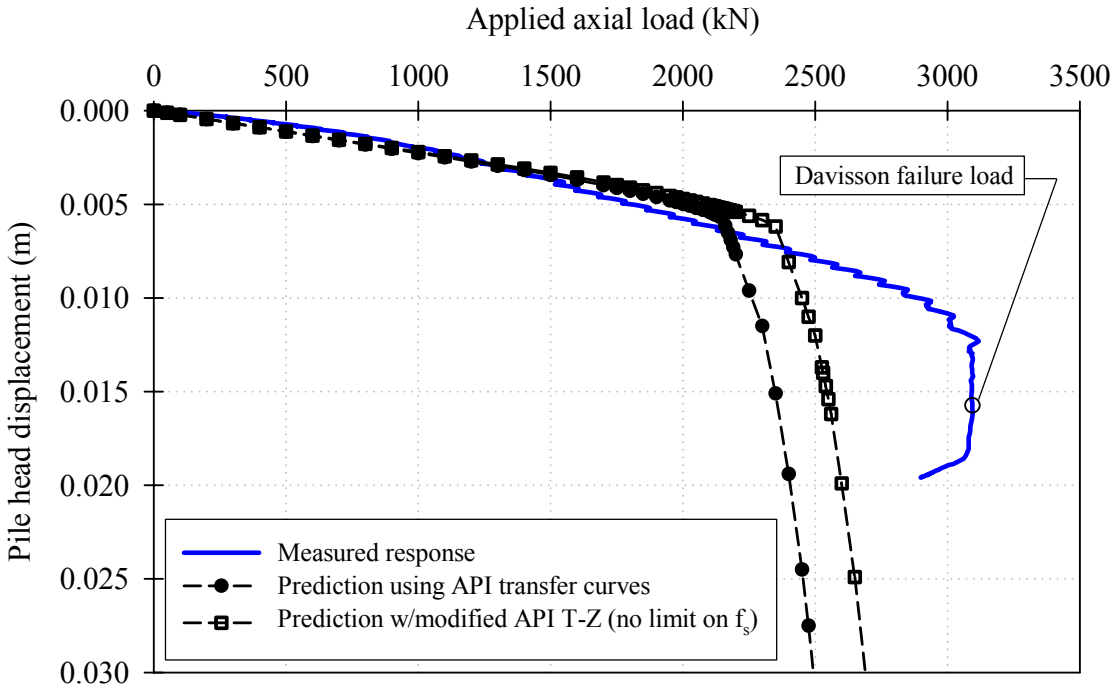


**Figure 7.13 Settlement predictions for the prestressed concrete pile using API (1993)**

#### 7.3.3.1.4 Prediction for the FRP test pile

The predicted load-settlement curves for the FRP test pile, using the API (1993) load transfer curves with and without a limiting shaft shear stress, are shown in Figure 7.14.

Figure 7.14 shows a good agreement for the initial portions of the predicted settlement curves and the measured load settlement curve. However, similar to the prestressed concrete pile predictions, the API prediction using an $f_s$ cutoff under-predicts the pile capacity and the onset of large settlements occurs at lower load than observed in the field measurements. The prediction with no $f_s$ cutoff shows a much better correspondence with the field measurements, but also shows the onset of large settlements occurring at a load slightly below the one measured in the field.

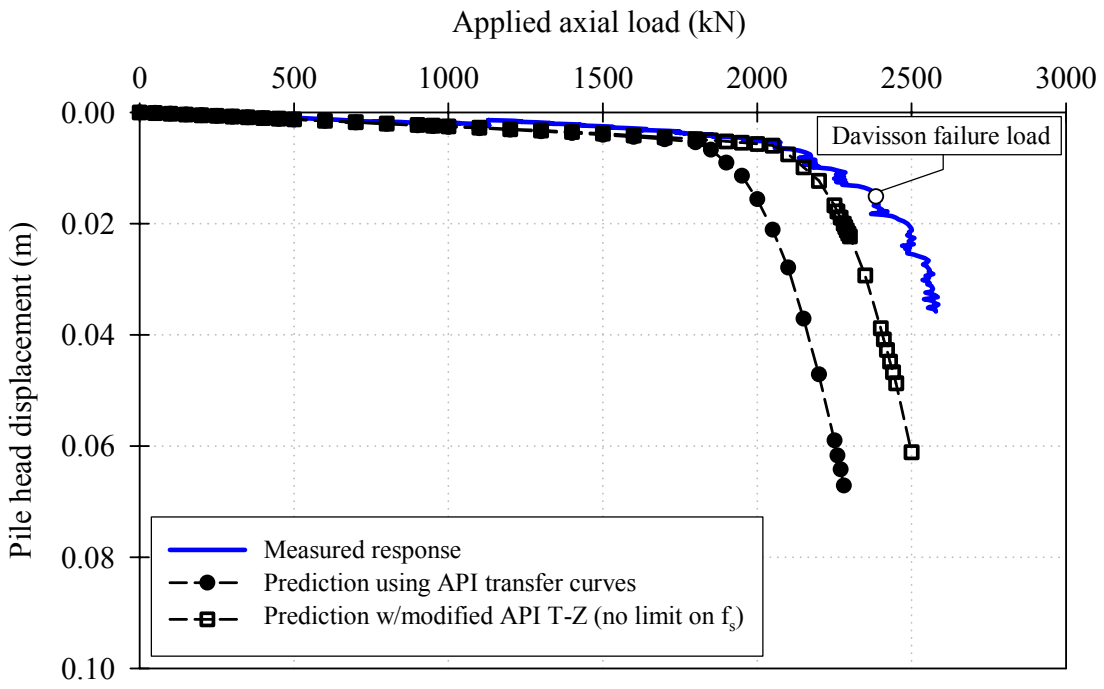


**Figure 7.14 Settlement predictions for the FRP pile using API (1993)**

#### 7.3.3.1.5 Prediction for plastic test pile

The predicted load-settlement curves for the plastic test pile, using the API (1993) load transfer curves with and without a limiting shaft shear stress, are shown in Figure 7.15.

Figure 7.15 shows that the predicted load-settlement curve, using API (1993) with a limiting $f_s$, agrees well with the initial portion of the field measurements, but large settlements start to occur sooner than observed at about 1700 kN. On the other hand, the API prediction using no $f_s$ cutoff shows very good agreement in both the initial and final portions of the settlement curve from the pile load test.

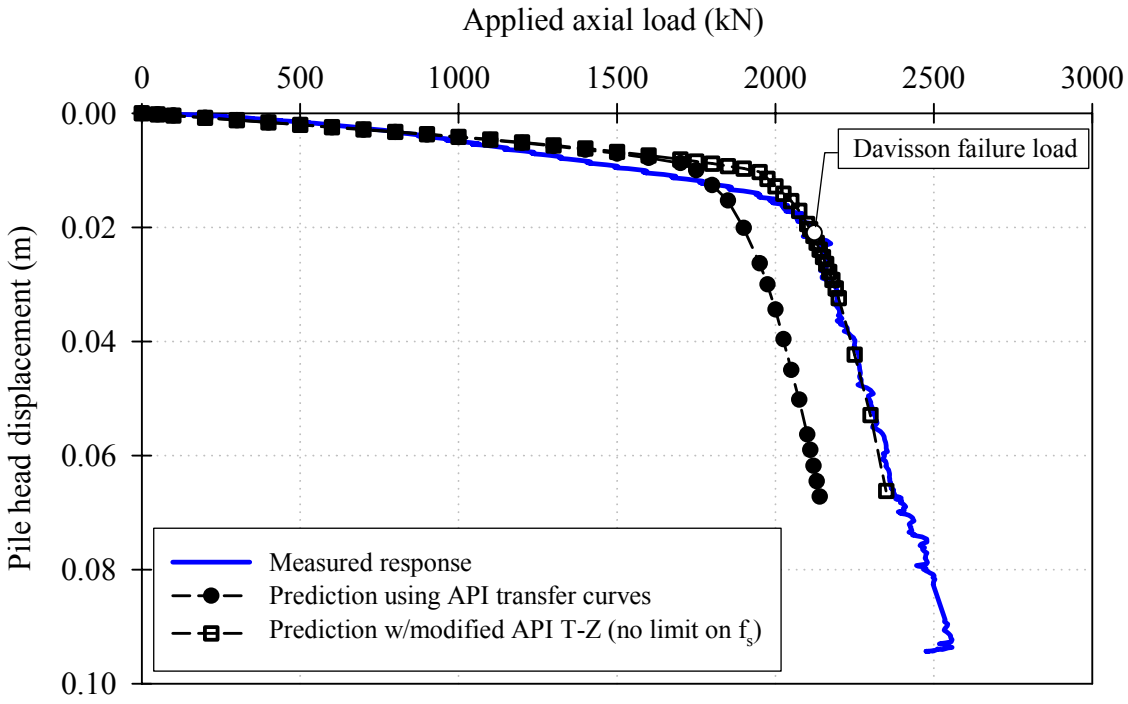


**Figure 7.15 Settlement predictions for the plastic pile using API (1993)**

### 7.3.3.2 Predictions using Vijayvergiya (1977) load transfer curves

#### 7.3.3.2.1 Load transfer curves recommended by Vijayvergiya (1977)

Vijayvergiya (1977) recommends the following load-transfer expression of mobilized unit side shear, $f_s$ as a function of shaft movement Z:

$$f_s = f_{s,max} \cdot \left( 2 \cdot \sqrt{\frac{z}{z_c}} - \frac{z}{z_c} \right) \text{ (for } z \le z_c \text{)}$$
$$f_s = f_{s,max} \text{ (for } z > z_c \text{)} \qquad (7.14)$$

where: $f_s$ = is the unit side shear stress mobilized along a pile segment at movement, z,
$f_{s,max}$ = is the maximum unit side shear stress,
z = movement of pile segment,
$z_c$ = movement required to mobilize $f_{s,max}$ (0.3 inches for sands)

The normalized T-Z curve obtained from Equation 7.14 is shown in Figure 7.16. For comparison purposes, the API T-Z curve is also shown in this figure.

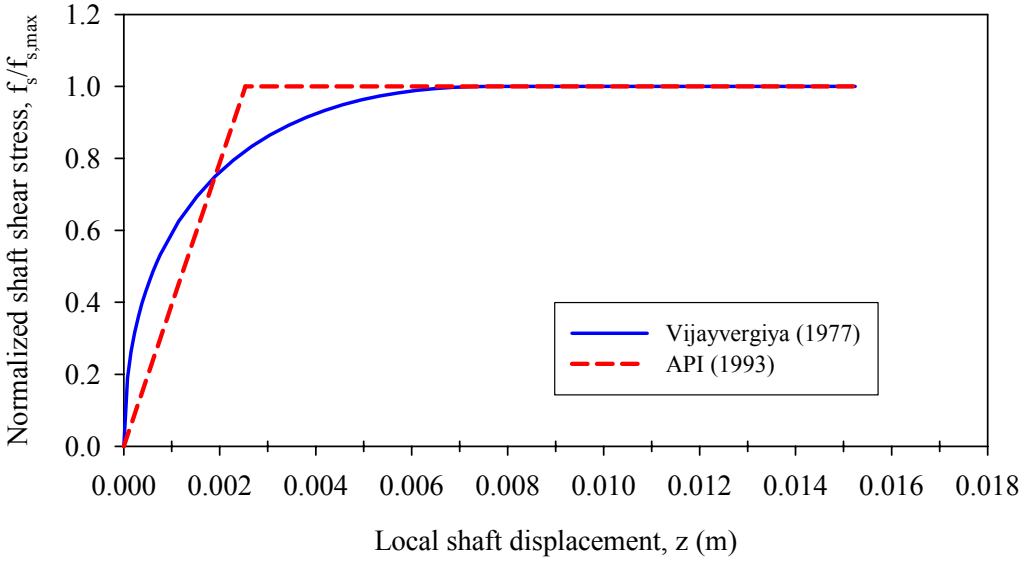


**Figure 7.16 Normalized T-Z curves according to API (1993) and Vijayvergiya (1977)**

Similarly, the following expression for pile tip load versus tip settlement for piles in sands is proposed by Vijayvergiya (1977):

$$q = \left(\frac{z}{z_c}\right)^{\frac{1}{3}} \cdot q_{max} \quad (\text{for } z \le z_c) \qquad (7.15)$$
$$q = q_{max} \quad (\text{for } z > z_c)$$

where: $q$ = is the pile tip resistance mobilized at displacement z,
$q_{max}$ = is the maximum tip resistance (end bearing),
z = movement of pile segment,
$z_c$ = movement required to mobilize $q_{max}$ (0.25 in. for sands).

The normalized Q-Z curve proposed by Vijayvergiya (1977) is shown in Figure 7.17. For comparison purposes, the corresponding API (1993) curve for a 24-inch diameter pile is also shown.

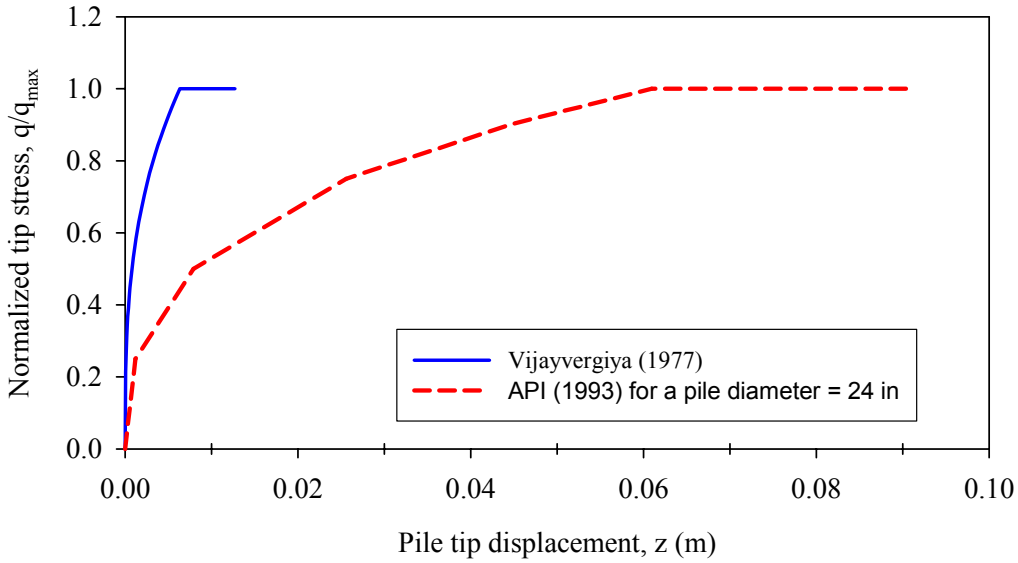


**Figure 7.17 Normalized Q-Z curves according to Vijayvergiya (1977) and API (1993)**

It is clear from Figure 7.17 that the Q-Z curve proposed by Vijayvergiya mobilizes the full end-bearing capacity at much smaller displacement than the API curve. Vijayvergiya (1977) estimates that about 0.25 inches (6.35 mm) of tip displacement are required to mobilize the ultimate pile end bearing, while API (1993) estimates a pile tip displacement equal to 10 % of the pile diameter is required.

#### 7.3.3.2.2 Maximum shaft shear stress distributions

Vijayergiya (1977) recommended using an expression similar to API (1993) to estimate the maximum shear stresses along the pile (See Equation 7.6). The author indicated that the coefficient of lateral earth pressures, K, can be as high as 1.25 for driven piles in medium dense to dense sand.

The predictions presented in the following subsections are based on shaft shear stresses calculated using Equation 7.6, with the δ values from the interface shear tests presented in Chapter 3, and K values of 1.0 and 1.25. The shear stress distributions used are shown in Figure 7.18. No limiting value of shear stress was used, although it should be pointed out that Vijayvergiya (1977) does mention the existence of a limiting value in the 1971 version of the API guidelines.

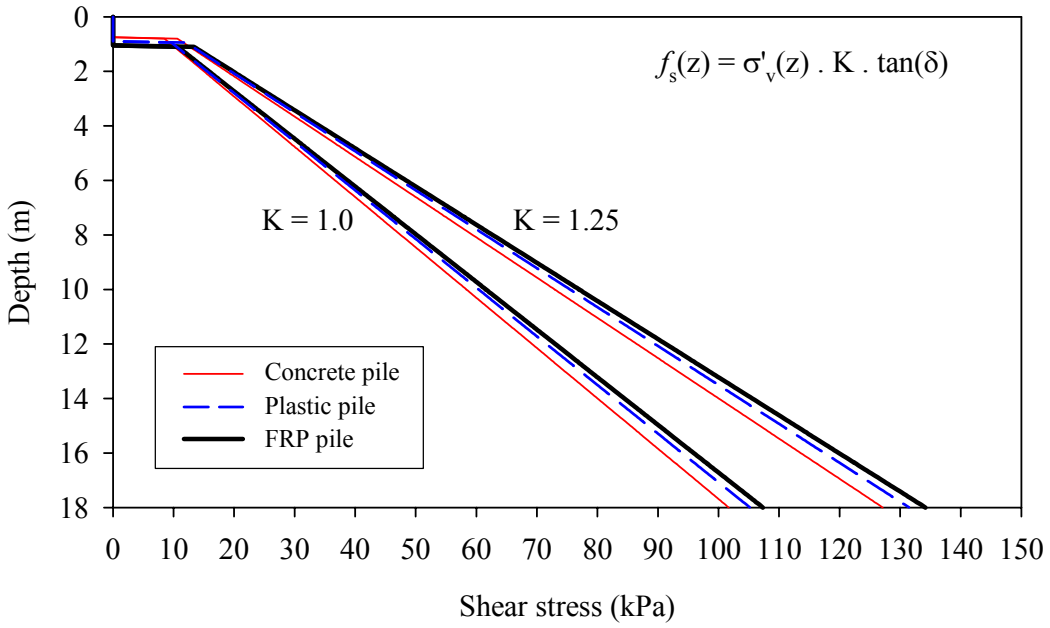


**Figure 7.18 Maximum shear stress distributions used in predictions using Vijayvergiya (1977)**

#### 7.3.3.2.3 Tip resistances

Vijayvergiya (1977) recommends estimating the tip resistance for piles driven in sands as the product of a bearing capacity factor, $N_q$, and the free-field effective overburden stress at the base of the pile, $\sigma'_v$.

The values recommended by API (1993) were used in the predictions presented in the following sections.

#### 7.3.3.2.4 Prediction for the prestressed concrete test pile

The predicted load-settlement curves for the prestressed concrete test pile, using the recommendations proposed by Vijayvergiya (1977) for load transfer curves are shown in Figure 7.19.

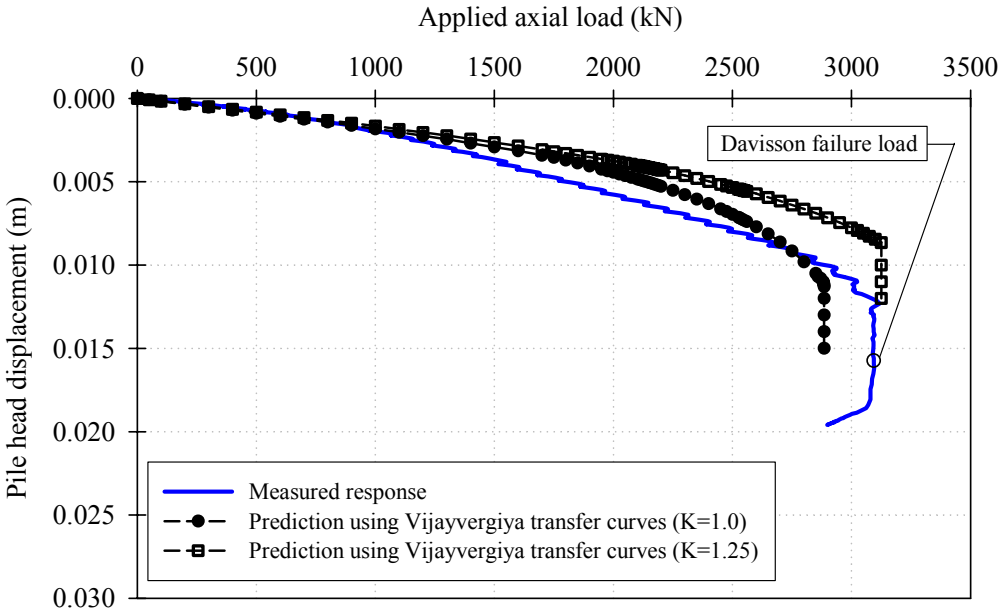


**Figure 7.19 Settlement predictions, for the concrete pile, using Vijayvergiya (1977)**

Figure 7.19 shows that the predicted load-settlement curve, using Vijayvergiya (1977), agrees well with the initial portion of the field measurements, but shows a stiffer response for loads higher than 1000 kN. The ultimate pile capacities predicted using coefficients of lateral earth pressures, K, of 1.0 and 1.25, were about 2885 kN, and 3125 kN. These capacities, as percentages of the pile capacity measured in the field, are about 93% and 101 % for K equal to 1.0 and 1.25, respectively.

#### 7.3.3.2.5 Prediction for the FRP test pile

The predicted load-settlement curve for the FRP test pile, using the Vijayvergiya (1977) load transfer curves, with a coefficient of lateral earth pressure, K = 1.0, is shown in Figure 7.20.

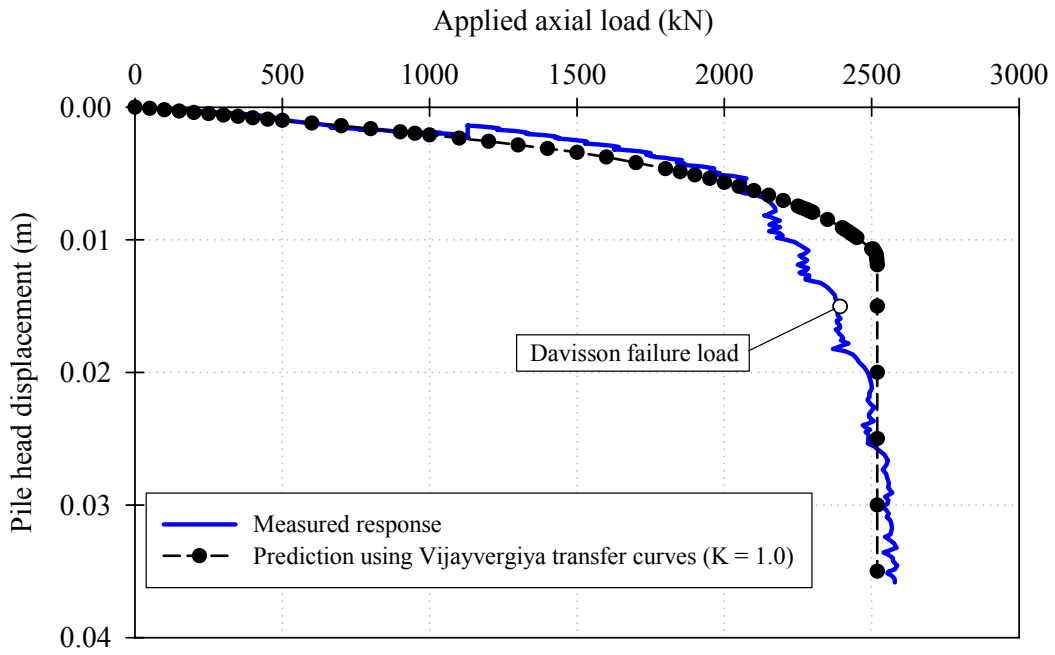


**Figure 7.20 Settlement predictions, for the FRP pile, using Vijayvergiya (1977)**

Figure 7.20 shows that the predicted load-settlement curve, using Vijayvergiya (1977) with a lateral earth pressure coefficient, K, equal to 1.0, agrees reasonably well with the field measurements.

#### 7.3.3.2.6 Prediction for the plastic test pile

The predicted load-settlement curve for the FRP test pile, using the Vijayvergiya (1977) load transfer curves, with K = 1.0, is shown in Figure 7.21.

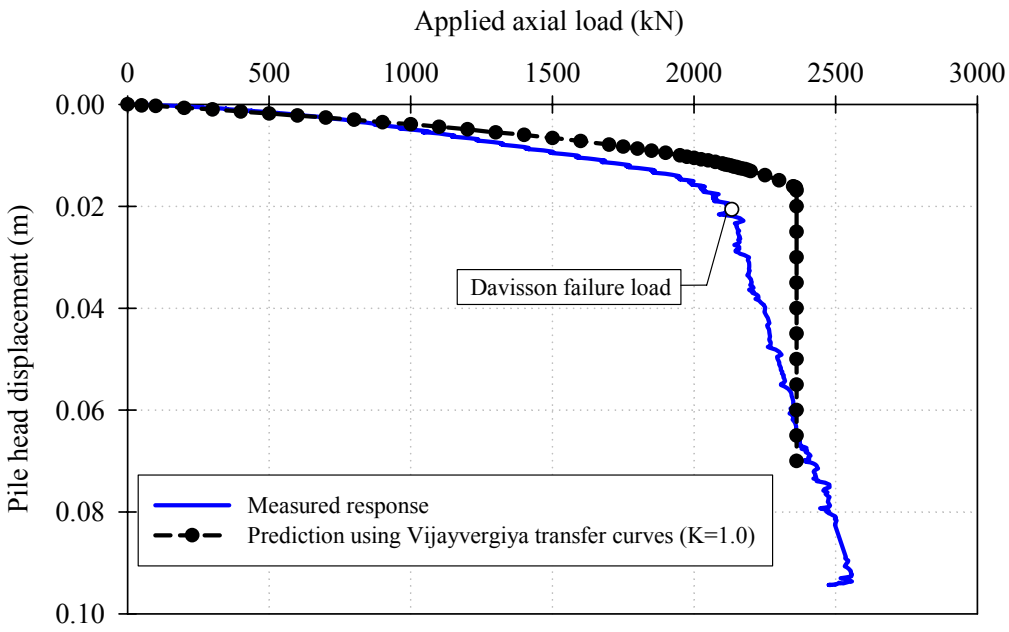


**Figure 7.21 Settlement predictions, for the Plastic pile, using Vijayvergiya (1977)**

Figure 7.21 shows that the predicted load-settlement curve, using Vijayvergiya (1977) with a lateral earth pressure coefficient, K, equal to 1.0, is stiffer than observed in the field.

#### 7.3.3.3 Comments on the predictions obtained using empirical load transfer curves

The exactness of load-settlement behavior predicted using the load-transfer (T-Z) method, will depend to a great extent on the accuracy of the predicted ultimate shaft and tip capacities (e.g., as presented in Section 7.2.2 for the API method), and on the displacement characteristics (e.g. stiffness, linear or non-linear, displacement required for full strength mobilization) chosen to model the soil-pile interface and the soil-pile tip during load transfer. For example, the results for the prestressed concrete pile, presented in the previous section for the API method, showed a significant under-prediction of the pile capacity. This is related to the low ultimate shaft resistance predicted compared to the actual ultimate shaft capacity recorded in the field. The prediction using Vijayvergiya (1977) with a coefficient of lateral earth pressure, K, of 1.25, was reasonably good. The predictions for the composite piles were more accurate

because the calculated ultimate shaft and tip capacities were much closer to the actual values measured.

### 7.3.4 Predictions using theoretical load transfer curves

The following sections present the background and describe the methodology used in this research to develop theoretically based load transfer curves. Most of the work in this area is based on the pioneering work by Kraft et al. (1981).

#### 7.3.4.1 Theoretical load transfer curves for a linear elastic soil

The soil deformation around a pile shaft can be idealized as concentric cylinders in shear (Frank 1974; Randolph and Wroth 1978). This idealization assumes the soil displacement due to the pile loads is predominantly vertical and that radial displacements are negligible. Studies by Frank (1974) and Baguelin et al. (1975) have shown that the concentric cylinder approach is a good approximation of the deformation patterns obtained using more rigorous analyses such as the finite element method.

Randolph and Wroth (1978) derived an expression for pile settlement in a linear elastic soil based on the concentric cylinder assumption. The author's derivation starts by first considering the vertical equilibrium of the annular shaped soil element (ring of soil between two concentric cylinders) shown in Figure 7.22:

$$\left(\tau + \frac{\partial \tau}{\partial r}\cdot dr\right)\cdot (r+dr)\cdot d\theta \cdot dy - \tau \cdot r \cdot d\theta \cdot dy + \\ +(\sigma_y + \frac{\partial \sigma_y}{\partial y}\cdot dy)\cdot (r+\frac{dr}{2})\cdot d\theta \cdot dr - \sigma_y \cdot (r+\frac{dr}{2})\cdot d\theta \cdot dr = 0 \qquad (7.16)$$

where the term definitions are shown in Figure 7.22. The vertical stress, $\sigma_y$, shown in this figure refers to net change in vertical stress due to the axial load, P, applied to the pile.

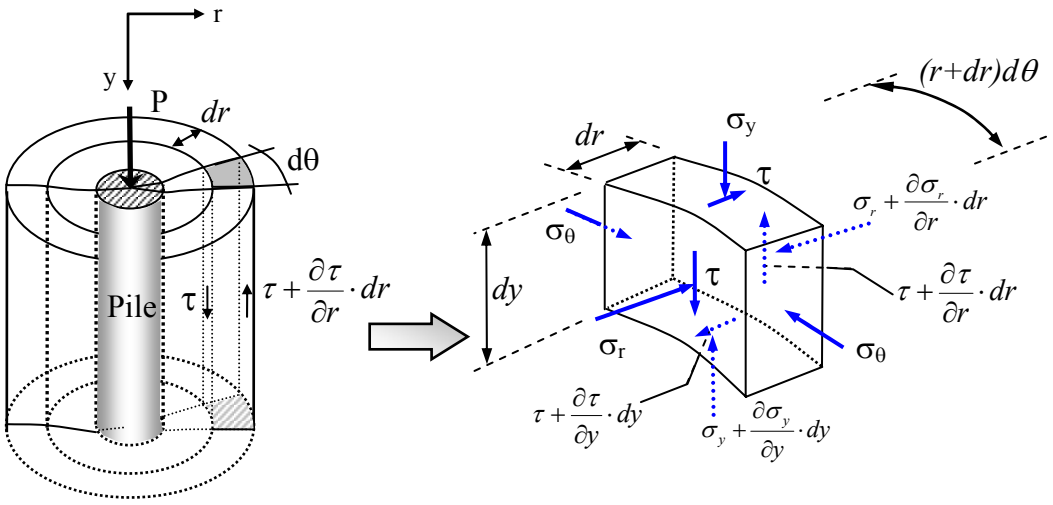


a) Concentric cylinders around loaded pile b) Stresses in soil element

**Figure 7.22 Concentric cylinder model for settlement analysis of axially loaded piles (adapted from Randolph and Wroth, 1978)**

Simplifying and neglecting second order terms, Equation 7.16 reduces to:

$$\frac{\partial(\tau \cdot r)}{\partial r} + r \cdot \frac{\partial \sigma_y}{\partial y} = 0 \qquad (7.17)$$

However, according to Randolph and Wroth (1978), the rate of change of vertical stress with respect to depth is much less than the rate of change of shear stress with respect to radial distance during axial loading of a pile. Therefore the second term of Equation 7.17 can be neglected, and the above equilibrium equation can be approximated as:

$$\frac{\partial(\tau \cdot r)}{\partial r} \approx 0 \qquad (7.18)$$

Integrating this last expression we obtain:

$$\int_{r_o}^{r} d(\tau \cdot r) = 0 \quad \Rightarrow \quad \left[\tau(r) \cdot r - \tau(r_o) \cdot r_o\right] = 0$$
$$\tau(r) = \frac{\tau(r_o) \cdot r_o}{r} = \frac{\tau_o \cdot r_o}{r} \tag{7.19}$$

where:

- $\tau(r)$ = shear stress acting at a radial distance r from the centerline of the pile,
- $\tau_o = \tau(r_o)$ = shear stress at the pile/soil interface (i.e. at a radial distance $r_o$),
- $r_o$ = pile radius (or equivalent radius for noncircular piles).

Equation 7.19 indicates that the shear stresses in the vicinity of the pile are inversely proportional to the radial distance to the pile.

The concentric cylinders model assumes that simple shear conditions prevail. This model also assumes that the radial displacements are negligible compared to the vertical displacements of the soil. Therefore the shear strain, $\gamma$, can be approximated as:

$$\gamma = \frac{\partial u}{\partial z} + \frac{\partial w}{\partial r} \approx \frac{dw}{dr} \tag{7.20}$$

where:

- u = radial displacement (neglected),
- w = vertical displacement.

For linear elastic soils, the shear strain is related to the shear stress as follows:

$$\gamma(r) = \frac{dw}{dr} = \frac{\tau(r)}{G(r)} \tag{7.21}$$

By substituting Equation 7.19 into Equation 7.21, we obtain:

$$\gamma(r) = \frac{dw}{dr} = \frac{\tau_o \cdot r_o}{r \cdot G(r)}$$
$$dw = \frac{\tau_o \cdot r_o}{G(r)} \cdot \frac{dr}{r} \qquad (7.22)$$

The settlement of the pile shaft, $w_s$, as originally proposed by Randolph and Wroth (1978), is obtained by integrating Equation 7.22 assuming a linear elastic soil with no radial variation of G (i.e., G(r) = G), as follows:

$$w_s = \tau_o \cdot r_o \cdot \int_{r_o}^{r_m} \frac{dr}{G \cdot r} = \frac{\tau_o \cdot r_o}{G} \cdot \ln\left(\frac{r_m}{r_o}\right) \qquad (7.23)$$

Where $r_m$ is the radial distance at which shear stresses in the soil become negligible. Randolph and Wroth (1978) suggested estimating $r_m$ using the following empirical expression:

$$r_m = 2.5 \cdot l \cdot \rho \cdot (1 - \upsilon) \qquad (7.24)$$

where:

- l = pile embedment depth,
- $\rho$ = factor of vertical homogeneity of soil stiffness = $\frac{G(\text{at pile mid-depth})}{G(\text{at pile tip})}$,
- $\upsilon$ = Poisson's ratio of the soil.

Equation 7.23, results in an equivalent linear "T-Z" load transfer curve as shown in Figure 7.23. The stiffness or slope of this "T-Z" curve is:

$$K_s = \frac{G}{r_o \cdot \ln\left(\frac{r_m}{r_o}\right)} \qquad (7.25)$$

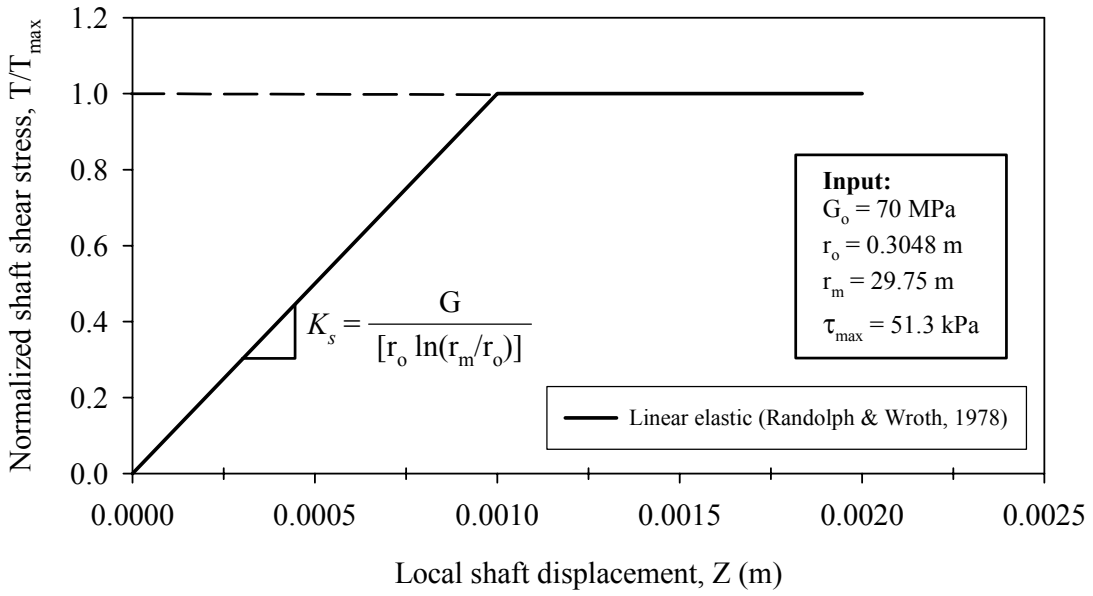


**Figure 7.23 Linear T-Z Curve obtained using Randolph and Wroth (1978)**

The value selected for $r_m$ has a large influence that on the resulting pile settlement. A recent study by Guo and Randolph (1999) used finite element and FLAC analyses to determine the value of $r_m$ more precisely. As a first approximation equation 7.24 provides reasonable values for $r_m$ (Randolph and Wroth 1978).

The load transfer curve for the pile tip can be approximated using Boussinesq's solution for a rigid footing resting on an elastic half-space (Poulos and Davis 1980):

$$Z_{base} = \frac{Q_b \cdot (1-\nu^2)}{2 \cdot E_s \cdot r_o} \tag{7.26}$$

where:

- $Q_b$ = The pile tip load,
- $E_s$, $\nu$ = Elastic modulus and Poisson's ratio of soil beneath pile tip,
- $r_o$ = pile radius.

The above equation can be expressed in terms of the shear modulus by substituting $E_s = 2 \cdot G \cdot (1+\nu)$ in Eq. 7.26:

$$Z_{base} = \frac{Q_b \cdot (1-\nu)}{4 \cdot G \cdot r_o} \tag{7.27}$$

The resulting $Q_b$-Z load transfer curve is shown in Figure 7.24.

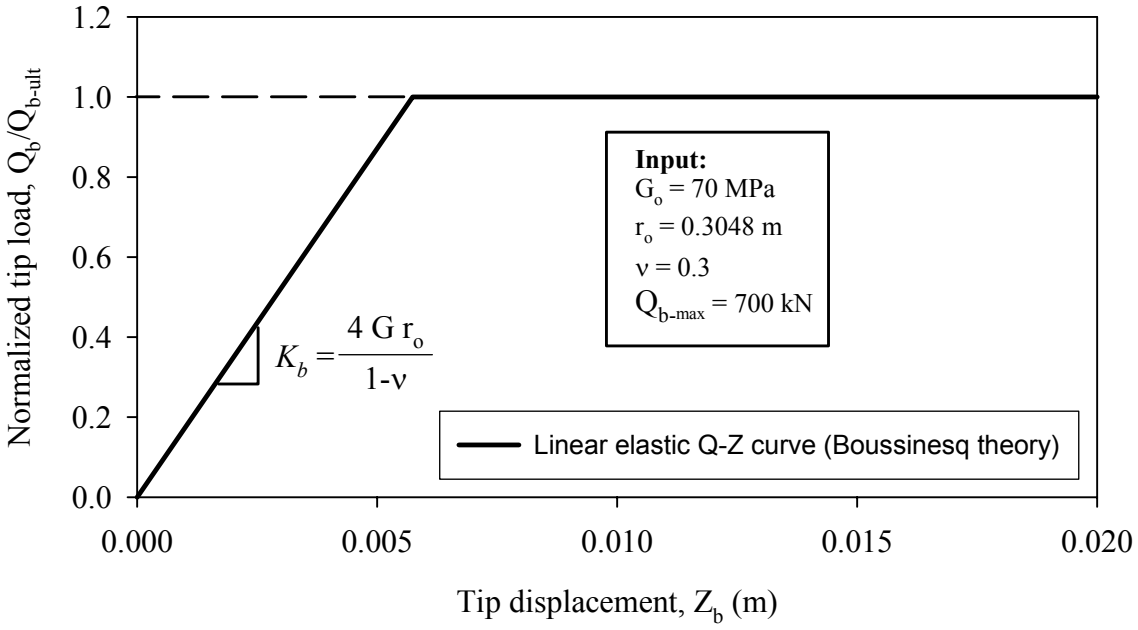


**Figure 7.24 Linear $Q_b$-Z curve obtained using Boussinesq's theory**

The slope of the linear $Q_b$-Z corresponds to the stiffness coefficient of the pile tip spring, and is given by:

$$K_{base} = \frac{4 \cdot G \cdot r_o}{(1-\nu)} \tag{7.28}$$

In the preceding derivations it was assumed that the soil is linear and elastic, with the parameters G and ν constant with both strain level and with radial distance from the pile. However, most soils exhibit stress-strain behavior that is highly non-linear and their stiffness can decay rapidly with strains (Atkinson, 2000). If settlement predictions are made using the above linear elastic load transfer curves, the appropriate elastic properties should be used. Poulos (2001) recommends using a secant shear modulus corresponding

to the load range applied to the pile. For the tip of a pile in sand, Poulos (2001) recommends increasing the shear modulus to account for soil densification below the pile tip due to driving. Successful application of a linear theory to a nonlinear problem requires judicious selection of elastic property values.

Non-linear load transfer curves that include soil nonlinearity are derived in the following subsections.

#### 7.3.4.2 Theoretical load transfer curves for a non-linear soil

##### 7.3.4.2.1 Initial shear modulus

As shown in Section 7.3.4.1, the shear stiffness of the soil deposit is a key property required in calculations of pile settlements. Sands typically only behave as linear elastic at very small shear strains of less than about 10 microstrains ($\gamma \leq 10^{-3}$ %). The shear modulus in this range of very small shear strains is often referred to as the "initial" "maximum" or "elastic" shear modulus. Here it will be referred to as the initial shear modulus, $G_o$. To perform non-linear pile settlement analyses, the initial shear modulus profile along the length of the pile must be estimated.

Elastic theory relates $G_o$ to the shear wave speed, $V_s$, as follows:

$$G_o = \rho \cdot V_s^2 \tag{7.29}$$

where $\rho$ is the soil mass density.

Therefore, the initial shear modulus could be obtained from in-situ measurements of the shear wave speed, such as from seismic CPT soundings. If seismic tests are not available, as is the case for the Route 351 site, $G_o$ can be estimated using empirical correlations with in-situ CPT tests (Lunne et al., 1997).

Several equations have been proposed to estimate $G_o$ from CPT $q_c$, some of the most important ones are:

- Baldi et al. (1989) from calibration chamber tests on uncemented, quartzitic sands:

$$\left(\frac{G_o}{q_c}\right)_{Average} = 1615 \cdot \left(\frac{q_c}{\sqrt{\sigma'_{vo}}}\right)^{-0.764} \tag{7.30}$$

Where $\sigma'_{vo}$ is the in-situ effective overburden pressure at the depth of $q_c$, and the units of $G_o$, $q_c$, and $\sigma'_{vo}$ are in kPa.

- Rix and Stokoe (1991) from calibration chamber tests on uncemented, quartzitic sands:

$$\left(\frac{G_o}{q_c}\right)_{Average} = 1634 \cdot \left(\frac{q_c}{\sqrt{\sigma'_{vo}}}\right)^{-0.75} \tag{7.31}$$

Where $\sigma'_{vo}$ is the in-situ effective overburden pressure at the depth of $q_c$, and where $G_o$, $q_c$, and $\sigma'_{vo}$ are in kPa.

- Equation 7.11, originally proposed by Chow (1996). Equation 7.11 is based on a re-interpretation of the calibration chamber tests run by Baldi et al. (1989):

$$G = \frac{q_c}{[A + B \cdot \eta - C \cdot \eta^2]}$$

and (7.11)

$$\eta = \frac{q_c}{\sqrt{P_a \cdot \sigma'_v}}$$

where: $q_c$ = CPT tip resistance,
$A = 0.0203$,
$B = 0.00125$,
$C = 1.216 \times 10^{-6}$,
$\sigma'_v$ = free-field effective overburden pressure,
$P_a$ = atmospheric pressure (100 kPa).

#### 7.3.4.2.2 Modeling soil nonlinearity using hyperbolic models

Hyperbolic stress-strain models have been found to adequately represent the non-linear behavior of most soils (Kondner 1963, Kondner and Zelasko 1963, Duncan and Chang 1970). Use of hyperbolic functions to model non-linear load-transfer functions for piles has been proposed by several researchers (e.g., Kraft et al. 1981; Chow 1986; McVay et al. 1989). The hyperbolic form of the shear stress-shear strain relationship is given by:

$$\tau = \frac{\gamma}{\frac{1}{G_o} + \frac{\gamma}{\tau_{ult}}} \tag{7.32}$$

where:

- $\gamma$ = shear strain,
- $G_o$ = initial tangent shear modulus,
- $\tau_{ult}$ = shear stress value that the hyperbola tends asymptotically (not to be confused with $\tau_{max}$),
- $\tau$ = shear stress value corresponding to strain, $\gamma$.

Duncan and Chang (1970) related the asymptotic value, $\tau_{ult}$, to the maximum shear stress, $\tau_{max}$, by:

$$\tau_{max} = R_f \cdot \tau_{ult} \tag{7.33}$$

Where $R_f$ is the failure ratio, and is typically a value less than or equal to one. For values of $R_f$ less than 1.0 the failure stress ($\tau_{max}$) is reached at a finite shear strain. For $R_f$ equal to 1.0 the failure stress would be reached asymptotically at a shear strain of infinity.

By substituting Equation 7.33 and $\tau = G_{sec} \cdot \gamma$ into Equation 7.32, we obtain the following expression for the secant shear modulus:

$$G_{sec} = G_o \cdot \left( 1 - \frac{\tau \cdot R_f}{\tau_{max}} \right) \tag{7.34}$$

If we include the radial variation of the shear stress, $\tau$, obtained earlier using the concentric cylinder assumption, i.e., by substituting Equation 7.19 into Equation 7.34:

$$G_{sec} = G_o \cdot \left( 1 - \frac{\frac{\tau_o \cdot r_o}{r} \cdot R_f}{\tau_{max}} \right) \tag{7.35}$$

Substituting the secant modulus $G_{sec}$ from Equation 7.35 into Equation 7.22, and evaluating the integral from radial distances $r_o$ to $r_m$, we obtain the following non-linear load-transfer (T-Z) relationship:

$$w_s = \frac{\tau_o \cdot r_o}{G_o} \cdot \ln \left( \frac{\frac{r_m}{r_o} - \frac{\tau_o \cdot R_f}{\tau_{max}}}{1 - \frac{\tau_o \cdot R_f}{\tau_{max}}} \right) \tag{7.36}$$

Equation 7.36, results in the "T-Z" load transfer curve shown in Figure 7.25. For comparison purposes the linear T-Z curve derived earlier is also shown. It can be seen that the initial stiffness or slope of the nonlinear "T-Z" curve is the same as the linear curve (Equation 7.25). The above equation becomes the linear elastic "T-Z" curve of Equation 7.23, when $R_f = 0$.

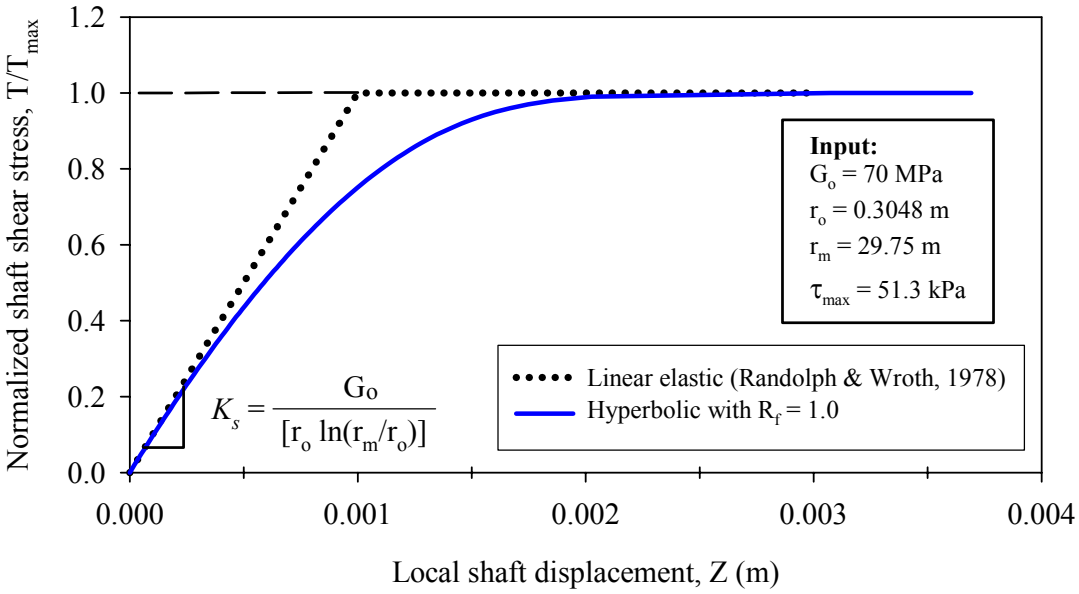


**Figure 7.25 Hyperbolic T-Z Curve based on Randolph and Wroth (1978)**

For the hyperbolic model, the relationship between the normalized secant shear modulus, $G_{sec}/G_o$, and the normalized shear stress, $\tau/\tau_{max}$, plots as a straight line with slope $-R_f$, as shown in Figure 7.26 (as given from Equation 7.34). Fahey and Carter (1993) and Fahey et al. (1994) showed that the hyperbolic model appropriately represented the shear modulus degradation observed in cyclic test data, but found that for monotonic tests, on both normally consolidated and overconsolidated sands, the shear modulus degraded at a much faster rate than suggested by the hyperbolic model. Randolph (1994) also pointed this out, and indicated that in practice, real soils often show a more rapid decay of the secant shear modulus with shear stress. This rapid reduction in $G_{sec}$ is observed when the very low strain initial shear modulus, obtained from dynamic tests, is used as initial reference (Randolph 1994, Atkinson, 2000). The value of the initial shear modulus measured using conventional laboratory tests is smaller than the "true" initial shear modulus at very small strains measured using dynamic measurements (Atkinson, 2000). The stiffness measured using conventional laboratory tests is lower because it is affected by factors such as: the quality of the soil sample, small disturbances during sample setup in the test apparatus, seating of loading platen, and small misalignments of loading ram (Atkinson, 2000). The conventional hyperbolic model may be more appropriate to capture the soil non-linearity when the initial modulus used is from conventional

laboratory tests. However, for initial soil modulus based on dynamic test measurements the modified hyperbolic model such as the one proposed by Fahey and Carter (1993) may be more suitable (Randolph, 1994).

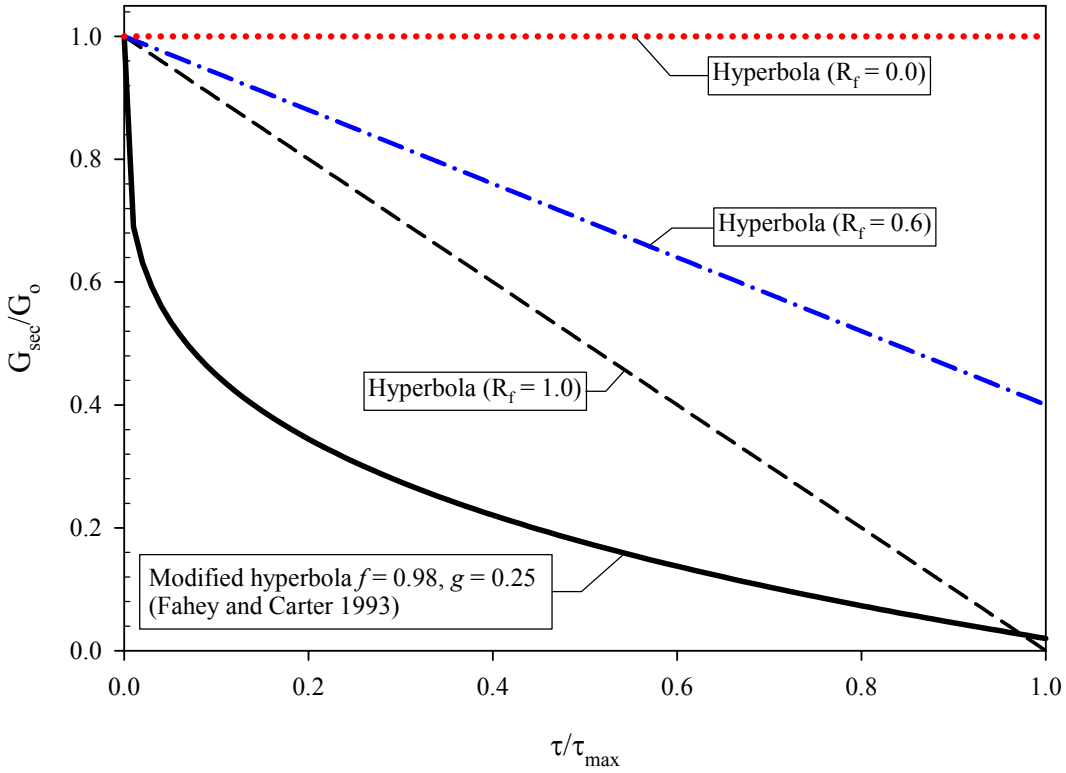


**Figure 7.26 Variation of secant shear modulus for different hyperbolic-type models**

To allow for a faster degradation of the secant shear modulus degradation, with respect to the "true" initial very low strain shear modulus, Fahey and Carter (1993) proposed using the following modified form of the hyperbolic expression:

$$\frac{G_{sec}}{G_o} = 1 - f \cdot \left( \frac{\tau}{\tau_{max}} \right)^g \qquad (7.37)$$

Where:

- $G_o$ = initial shear modulus (for shear strains below $10^{-5}$),
- $G_{sec}$ = secant shear modulus,

- $\tau$ = current shear stress,
- $\tau_{max}$ = maximum shear stress,
- $f$, $g$ = empirical curve fitting parameters.

Equation 7.37 becomes the standard hyperbolic model for $f = R_f$ and $g = 1$. Fahey and Carter (1993) found that the values of $f$ of 0.98 and $g$ of 0.25 gave a good fit for normally consolidated Toyoura sand. Toyoura sand is the Japanese standard sand, and it consists of a subangular fine sand, with a mean particle size, $D_{50}$ of 0.17 mm (Ishihara, 1996). This sand has characteristics similar to the in-situ sand at the Route 351 project. The nonlinear T-Z curve, corresponding to the Fahey and Carter (1993) modified hyperbolic $G_{sec}$ curve, can be easily derived using the same procedure as before. This expression is as follows:

$$w_s = \frac{\tau_o \cdot r_o}{G_o \cdot g} \cdot \ln \left( \frac{\left( \frac{r_m}{r_o} \right)^g - f \cdot \left( \frac{\tau_o}{\tau_{max}} \right)^g}{1 - f \cdot \left( \frac{\tau_o}{\tau_{max}} \right)^g} \right) \tag{7.38}$$

Equation 7.38 becomes Equation 7.36 (which corresponds to the conventional hyperbolic curve) when $f = R_f$ and $g = 1$. The T-Z curve obtained using Equation 7.38, and $f = 0.98$ and $g = 0.25$ is shown in Figure 7.27. As shown in Figure 7.27, the initial stiffness, $K_s$, of this T-Z curve is the same as the other two (since $K_s$ depends only on $G_o$, $r_o$, and $r_m$), but this curve degrades at a much faster rate than the one based on the conventional hyperbolic equation.

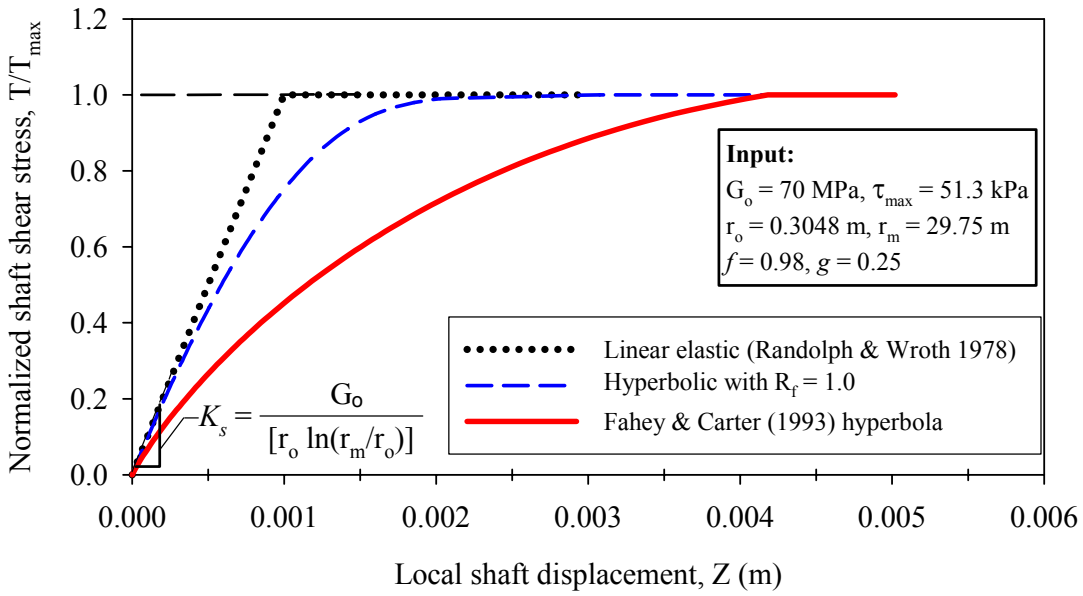


**Figure 7.27 Theoretically derived T-Z curve using concentric cylinders, and the modified hyperbola from Fahey and Carter (1993).**

So far we have only dealt with the side shear load transfer curves (T-Z curves). Because the nature of the shear strain distribution below a pile tip is more complex it is not as straight forward to model soil non-linearity for Q-Z curves as it was for the T-Z curves. An initial approximation consists of assuming a hyperbolic variation of the stiffness coefficient of the pile tip spring such as proposed by Chow (1986):

$$K_{secant}^{base} = K_{o}^{base} \times \left[ 1 - f \cdot \left( \frac{Q_b}{Q_{b\text{-}max}} \right)^{g} \right] \tag{7.39}$$

Where $K_o^{base}$ is equal to $K_{base}$ from Equation 7.28 (linear elastic soil case). The expression for the load transfer curve is:

$$Z_{base} = \frac{Q_b}{K_o^{base} \cdot \left[ 1 - f \cdot \left( \frac{Q_b}{Q_{b\text{-}max}} \right)^{g} \right]} \tag{7.40}$$

The $Q_b$-Z load transfer curve obtained using the above equation is shown in Figure 7.28. For comparison purposes the linear-elastic curve is also shown.

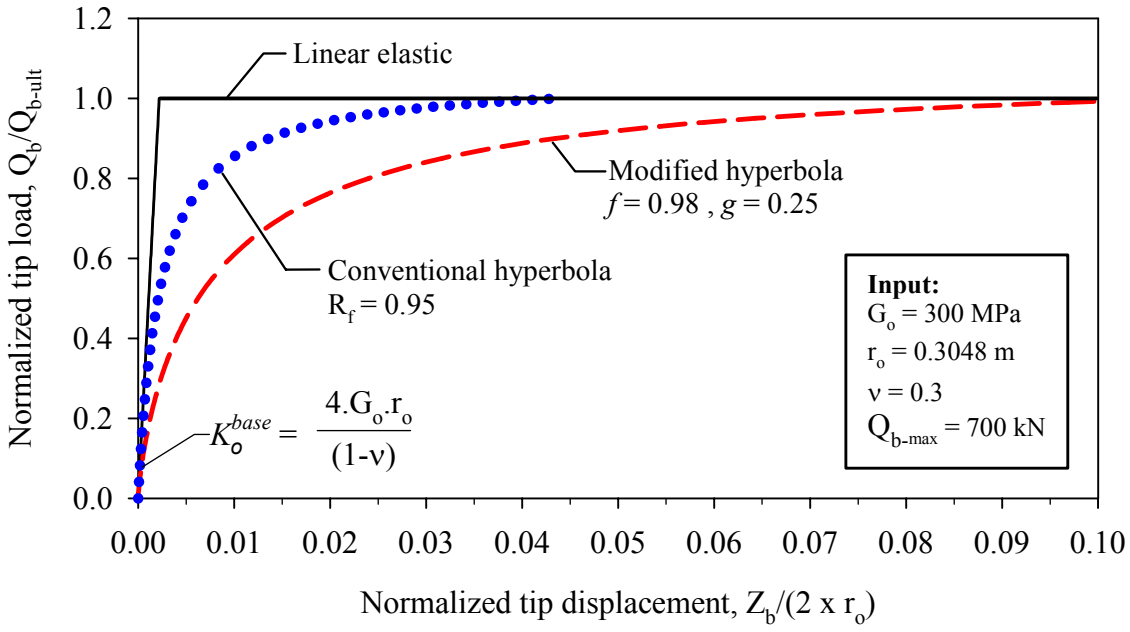


**Figure 7.28 Theoretically derived Q-Z curve using Boussinesq's theory, and the modified hyperbola from Fahey and Carter (1993).**

As shown in Figure 7.28, the ultimate tip resistance is developed at tip displacements of about 0.22 %, 4.4 %, and 10 %, for the load transfer curves based on the linear elastic, conventional hyperbolic ($R_f = 0.95$), and modified hyperbolic ($f = 0.98$, $g = 0.25$) models respectively. The very small peak tip displacement in the linear elastic load transfer curve is related to the use of the very low strain initial shear modulus. As mentioned earlier, use of a secant modulus is recommend to obtain more realistic displacements when using a linear elastic theory.

### 7.3.4.3 Input parameters used for the analyses of Route 351 using modified hyperbola theoretical load transfer curves

To analyze the piles tested at the Route 351 project using the modified hyperbolic load transfer curves derived above, adequate values for the initial shear modulus (for shaft and

base), and the maximum loads for the load transfer curves (i.e. the maximum shear stress for the shaft T-Z, and maximum end bearing pressure for the pile tip Q-Z) must be selected. The following subsections describe this selection process in detail.

#### 7.3.4.3.1 Hyperbola parameters

Based on the characteristics of the sands encountered at the test site modified hyperbola parameters of f = 0.98 and g = 0.25 were used.

#### 7.3.4.3.2 Initial shear modulus

The profiles of initial shear modulus obtained using the above equations 7.11, 7.30, and 7.31, and the design CPT profile for the Route 351 (Figure 7.2), are shown in Figure 7.29.

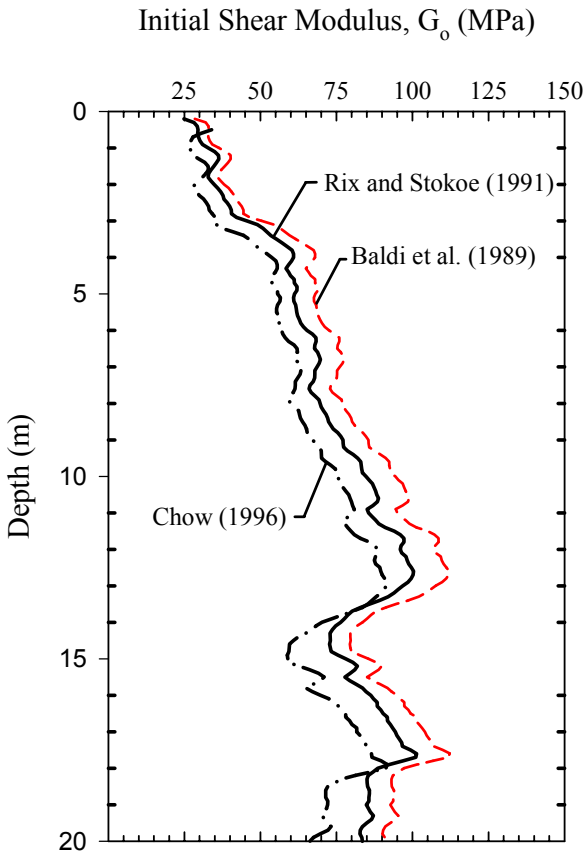


**Figure 7.29 Route 351 Initial Shear Modulus Profile from CPT Correlations**

Both the magnitude and distribution (radially and with depth) are important. Poulos (2001) distinguished the following different values of the shear modulus required for settlement calculations of single piles:

- The value of $G_o$ in the vicinity of the pile shaft. This value will strongly influence the settlement of the pile.
- The value of $G_o$ immediately below the pile tip.

Pile installation will greatly affect the shear modulus values in a zone near the pile (Poulos, 1988). For driven piles in sands, the stiffness may actually be higher than the in-situ value of the soil mass prior to pile installation (Randolph, 1994). During pile installation the increase of radial stresses and associated densification will tend to increase the soil shear modulus, however a competing effect which tends to reduce the shear modulus is the induced shear strains. The effects of pile installation on the magnitude and distribution of $G_o$ are difficult to quantify. If the installation effects are known, Kraft et al. (1981) and Randolph (1994) presented procedures to include the radial variation of shear modulus in the theoretical load transfer curves. However, they both considered the installation effects less important than the nonlinear effects and generally minor compared to the uncertainties involved in the estimated soil properties. Therefore, the analyses presented in the following sections are based on the $G_o$ profile presented in Figure 7.29, but for the pile tip the $G_o$ value selected was based on an average of the in-situ $G_o$ values measured immediately below the pile tip times a factor of 4. This factor of 4 is used to account for sand densification below the pile tip. Poulos (2001) recommends increasing the in-situ stiffness immediately below the tip of driven piles in sands by a factor between 3 and 5.

#### 7.3.4.3.3 Maximum shear stresses

The maximum shear stresses are estimated using Equation 7.6, using the interface friction angles obtained from interface friction tests. The coefficient of horizontal earth pressure, *K*, is assumed to range between 1.0 and 1.25. The range selected for *K* is consistent with the values recommended in the literature for displacement piles driven in sands (Bowles 1996, Poulos 2001).

#### 7.3.4.3.4 Ultimate tip resistance

The theoretical $Q_b$-Z curves require as input, in addition to the initial shear modulus and the Poisson's ratio for the soil, the ultimate tip resistance, $Q_{b\text{-}max}$. For the predictions presented in the following sections, the $Q_{b\text{-}max}$ values were selected from the Imperial College method estimates presented earlier (Table 7.5). $Q_{b\text{-}max}$ values from other prediction methods could have been used, but the IC method had the closest toe capacity predictions.

### 7.3.4.4 Prediction for the concrete test pile

The predicted load-settlement curves for the prestressed concrete test pile, using the proposed theoretically derived load transfer curves are shown in Figure 7.30.

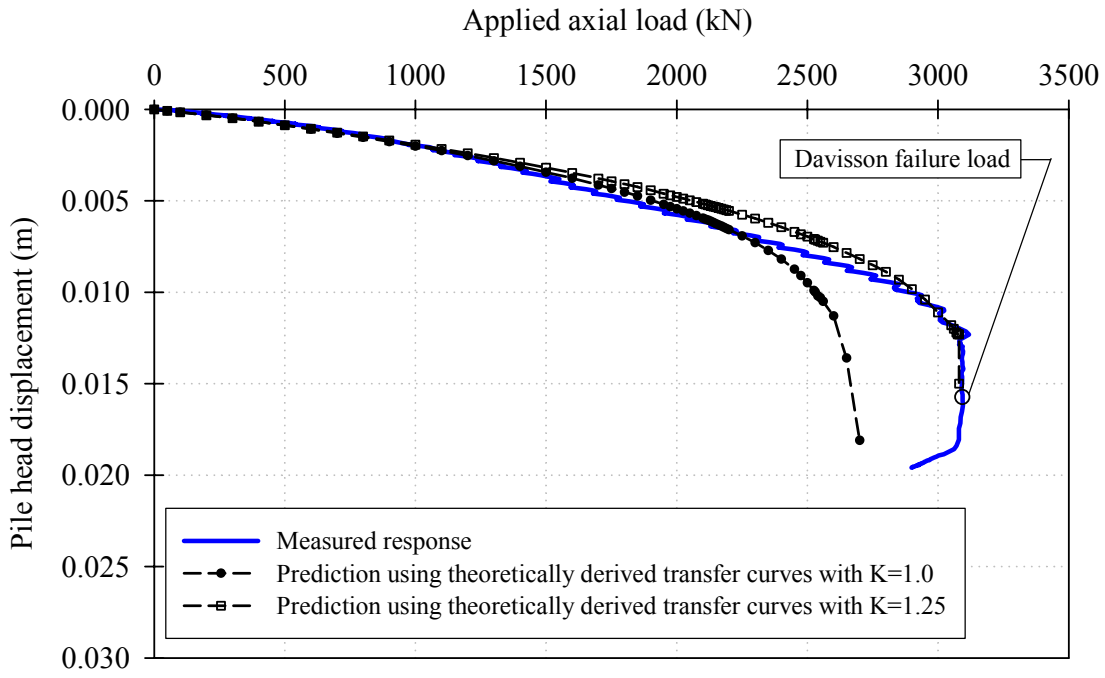


**Figure 7.30 Settlement predictions for the concrete pile using theoretically derived transfer curves**

Figure 7.30 shows that the predicted load-settlement curve, using the theoretically derived load transfer curves derived in the preceding section, and using the maximum

shear stresses calculated using a coefficient of horizontal earth pressures, K, of 1.25, is in reasonably good agreement with the measured performed. The analysis with K = 1.25, predicts the initial slope of the load-settlement curve and ultimate pile capacity quite well, but shows a slightly stiffer response for loads between 1500 and 2900 kN.

#### 7.3.4.5 Prediction for the FRP test pile

Using the proposed theoretically derived load transfer curves, and a value for K of 1.0, the load-settlement curve for the FRP test pile was predicted, as shown in Figure 7.31.

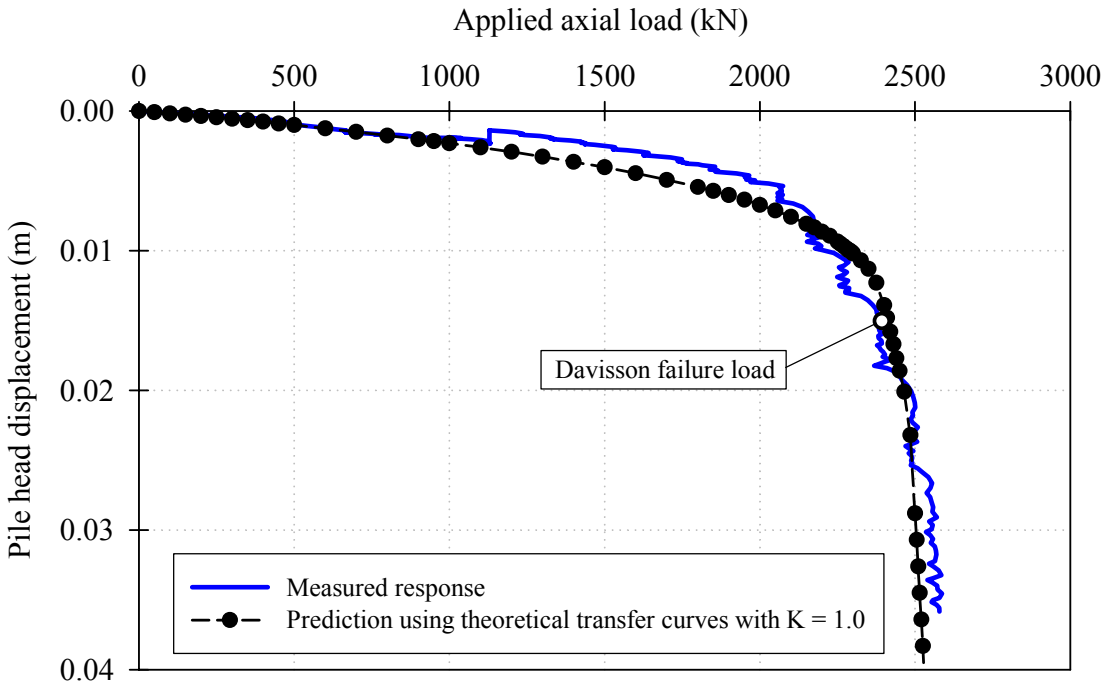


**Figure 7.31 Settlement prediction for the FRP pile using theoretically derived transfer curves**

Figure 7.31 shows a good agreement between the predicted load-settlement curve and the measured response.

### 7.3.4.6 Prediction for the Plastic test pile

The predicted load-settlement curves for the prestressed concrete test pile, using the proposed theoretically derived load transfer curves are shown in Figure 7.32.

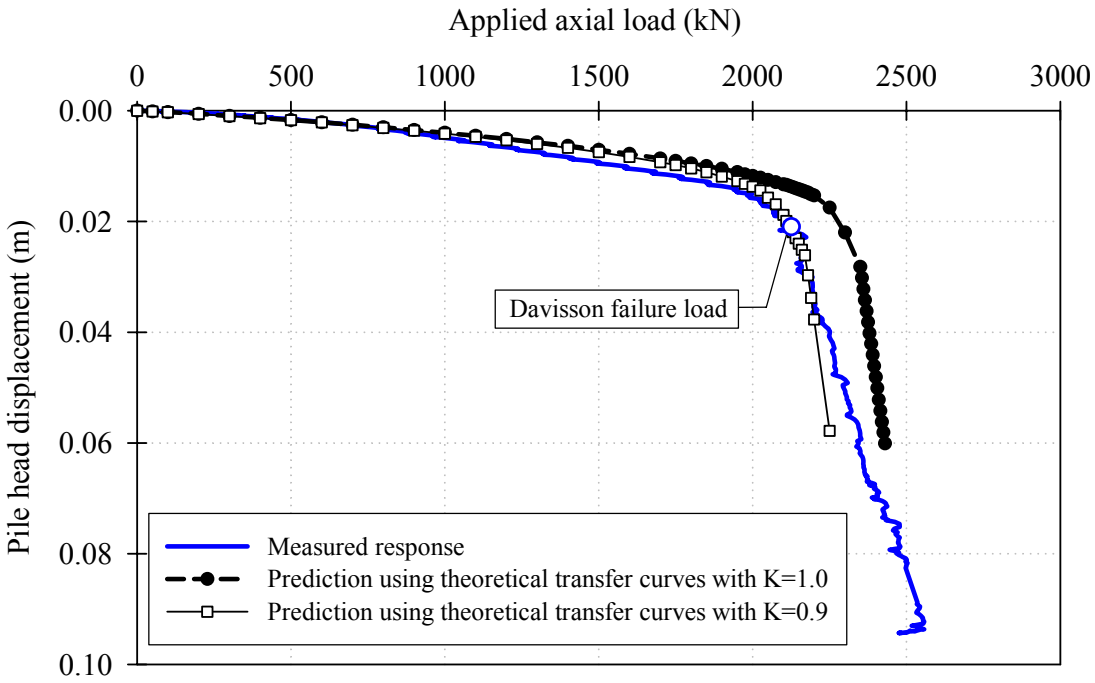


**Figure 7.32 Settlement predictions for the plastic pile using theoretically derived transfer curves**

Figure 7.32 shows that the predicted load-settlement curve, using the theoretically derived load transfer curves derived in the preceding section, and using the maximum shear stresses calculated using values of the coefficient of horizontal earth pressures, K, of 0.90 and 1.00. The analysis with K = 0.9 predicts well the initial slope of the load-settlement curve and load at which the steep change of slope occurs. However, neither of the analysis captures the slope of the second portion of the curve.

### 7.3.4.7 Comments on the predictions using theoretical load transfer curves

The predictions obtained using the theoretically derived load transfer curves were in very good agreement with the measured field behavior. The best agreements were found for

values of the coefficient of horizontal earth pressures, K, of 1.25, 1.0, and 0.9 for the prestressed concrete, FRP, and plastic piles, respectively. These differences in the K coefficient values are contrary to the expected outcome. The expected outcome was to have similar K values for the three test piles since they were installed in similar soil conditions, and they all are full displacement piles with similar cross sectional dimensions. It is possible that this is again related to the δ values measured in the laboratory not being representative of field conditions, perhaps due to the small displacements used in the lab of only 0.5 inches.

### 7.3.5 Residual stresses

The analyses presented in this chapter did not include the effects of residual stresses, although their importance in obtaining more accurate predictions is recognized. Based on the small level of residual stresses measured in the field (see Chapter 6), the effects of residual stresses were not considered. The impact of not incorporating residual stress effects would likely affect stiffness in the pile response rather than ultimate capacity.

## 7.4 CONCLUSIONS

The axial capacities of the three test piles were predicted using static analysis methods commonly employed in practice. The methods employed were the Nordlund method, the API method, the LCPC method, and the Imperial College method. The various methods used to predict axial pile capacity led to ratios of calculated to measured pile capacities ranging from 0.70 to 1.14 for the prestressed concrete pile, and from 0.81 to 1.33 for the composite piles. It was found that the level of accuracy of the predictions was comparable for all three test piles.

The prediction results seem to indicate that conventional static analysis methods are applicable to composite piles. However it is the author's opinion that additional case histories are needed to corroborate and extend this conclusion to other composite pile types and to different soil conditions.

The load-settlement behavior was predicted using t-z analyses. A series of these analyses were carried out to determine the adequacy of this method to analyze axially loaded composite pile types such as the ones studied in this research project. The analyses were completed using empirical load transfer curves available in the literature (e.g., API 1993, and Vijayvergiya 1977), and using theoretically derived load transfer curves.

The predictions using the empirical load transfer curves showed reasonable agreement with the field measurements for the composite piles. The predictions for the prestressed concrete pile showed less agreement and tended to underestimate the measured pile capacity. This could be related to the value of the interface friction angle used. The calculations were based on the interface friction angle measured in the lab, which may be inadequate to represent the field conditions experience by the pile, e.g., in the field the pile interface experienced much larger relative displacements compared to the 0.5 inches used in the laboratory.

The predictions obtained using the theoretically derived load transfer curves were in very good agreement with the measured field behavior. However, the values of the coefficient of horizontal earth pressures, K, which resulted in the best matches with field behavior, were 1.25, 1.0, and 0.9 for the prestressed concrete, FRP, and plastic piles, respectively. The differences in the K coefficient values are contrary to the expected outcome. The expected outcome was to have similar K values for the three test piles since they were installed in similar soil conditions, and they all are full displacement piles with similar cross sectional dimensions. It is possible that this is again related to the $\delta$ values measured in the laboratory not being representative of field conditions, perhaps due to the small displacements used in the lab of only 0.5 inches.

The prediction results seem to indicate that conventional t-z analyses are applicable to composite piles. However it is believed that additional case histories are needed to corroborate and extend this conclusion to other composite pile types and to different soil conditions.